JCI The Journal of Clinical Investigation

Viral acute lower respiratory infections impair CD8+ T cells through PD-1

John J. Erickson, … , Sebastian Joyce, John V. Williams

J Clin Invest. 2012;122(8):2967-2982. https://doi.org/10.1172/JCI62860.

Research Article Immunology

Viruses are leading causes of severe acute lower respiratory infections (LRIs). These infections evoke incomplete immunity, as individuals can be repeatedly reinfected throughout life. We report that acute viral LRI causes rapid pulmonary $CD8^+$ cytotoxic T lymphocyte (T_{CD8}) functional impairment via programmed death–1/programmed death ligand–1 (PD-1/PD-L1) signaling, a pathway previously associated with prolonged antigenic stimulation during chronic infections and cancer. PD-1–mediated T_{CD8} impairment occurred acutely in mice following infection with human metapneumovirus or influenza virus. Viral antigen was sufficient for PD-1 upregulation, but induction of PD-L1 was required for impairment. During secondary viral infection or epitope-only challenge, memory T_{CD8} rapidly reexpressed PD-1 and exhibited severe functional impairment. Inhibition of PD-1 signaling using monoclonal antibody blockade prevented T_{CD8} impairment, reduced viral titers during primary infection, and enhanced protection of immunized mice against challenge infection. Additionally, PD-1 and PD-L1 were upregulated in the lungs of patients with 2009 H1N1 influenza virus, respiratory syncytial virus, or parainfluenza virus infection. These results indicate that PD-1 mediates T_{CD8} functional impairment during acute viral infection and may contribute to recurrent viral LRIs. Therefore, the PD-1/PD-L1 pathway may represent a therapeutic target in the treatment of respiratory viruses.

Viral acute lower respiratory infections impair CD8+ T cells through PD-1

John J. Erickson,[1] Pavlo Gilchuk,[1] Andrew K. Hastings,[1] Sharon J. Tollefson,[2] Monika Johnson,[1] Melissa B. Downing,[1] Kelli L. Boyd,[1] Joyce E. Johnson,[1] Annette S. Kim,[1] Sebastian Joyce,[1] and John V. Williams[1,2]

[1]Department of Pathology, Microbiology, and Immunology and [2]Department of Pediatrics, Vanderbilt University School of Medicine, Nashville, Tennessee, USA.

Viruses are leading causes of severe acute lower respiratory infections (LRIs). These infections evoke incomplete immunity, as individuals can be repeatedly reinfected throughout life. We report that acute viral LRI causes rapid pulmonary CD8+ cytotoxic T lymphocyte (T_{CD8}) functional impairment via programmed death–1/programmed death ligand–1 (PD-1/PD-L1) signaling, a pathway previously associated with prolonged antigenic stimulation during chronic infections and cancer. PD-1–mediated T_{CD8} impairment occurred acutely in mice following infection with human metapneumovirus or influenza virus. Viral antigen was sufficient for PD-1 upregulation, but induction of PD-L1 was required for impairment. During secondary viral infection or epitope-only challenge, memory T_{CD8} rapidly reexpressed PD-1 and exhibited severe functional impairment. Inhibition of PD-1 signaling using monoclonal antibody blockade prevented T_{CD8} impairment, reduced viral titers during primary infection, and enhanced protection of immunized mice against challenge infection. Additionally, PD-1 and PD-L1 were upregulated in the lungs of patients with 2009 H1N1 influenza virus, respiratory syncytial virus, or parainfluenza virus infection. These results indicate that PD-1 mediates T_{CD8} functional impairment during acute viral infection and may contribute to recurrent viral LRIs. Therefore, the PD-1/PD-L1 pathway may represent a therapeutic target in the treatment of respiratory viruses.

Introduction

Human metapneumovirus (HMPV), respiratory syncytial virus (RSV), and influenza A virus (IAV) are leading causes of acute lower respiratory infection (LRI) worldwide, especially in infants, the elderly, and the immunocompromised (1–4). No effective vaccines or therapeutics exist for either HMPV or RSV, and influenza vaccine must be re-administered annually. Despite the frequency of infection with these viruses and minimal antigenic drift of HMPV and RSV, protective immunity is poorly established, as individuals can be repeatedly reinfected throughout life (5–7). An ineffective adaptive immune response might account for this susceptibility, as recent studies have demonstrated that infection of mice with RSV (8–11), IAV (9), or parainfluenza virus 5 (PIV-5) (12) results in impairment of pulmonary CD8+ cytotoxic T lymphocytes (T_{CD8}), cells that normally mediate recovery from LRI by elaboration of cytokines and direct lysis of infected cells (13). Specific mechanisms governing pulmonary T_{CD8} functional impairment during acute viral LRI remain incompletely defined and represent a potential avenue for therapeutic intervention and design of more effective vaccines.

T_{CD8} functions are tightly regulated by a variety of stimulatory and inhibitory receptors (14–16). During chronic infections (17–21) and cancer (22–24), programmed death–1 (PD-1) has a well-defined role in mediating T_{CD8} exhaustion, during which prolonged TCR stimulation by persistent viral or tumor antigens maintains PD-1 expression. PD-L1, a ligand for PD-1, is constitutively expressed by many hematopoietic cells and inducible on most other cell types by proinflammatory cytokines (25–27), including respiratory epithelial cells (27). PD-L1 ligation of PD-1 antagonizes TCR signaling by blocking PI3K/Akt activation, leading to reduced cytokine production, proliferation, and survival (28). Blocking PD-1 ligation restores function to exhausted T_{CD8} during HIV infection (19, 29), and recent clinical trials indicate that anti–PD-1 monoclonal antibody therapy is safe and at least partially effective against both refractory hematological malignancies (30) and solid tumors (31). Direct modulation of the PD-1/PD-L1 pathway therefore holds significant therapeutic potential.

A role for PD-1 in mediating T_{CD8} impairment during acute infections is unclear. Mice acutely infected with lymphocytic choriomeningitis virus (LCMV) have functional T_{CD8} that rapidly downregulate PD-1 in the infected spleen (17, 19), while mice acutely infected with Friend retrovirus have T_{CD8} that express high levels of PD-1 yet remain cytotoxic (32). In humans during acute hepatitis B virus infection, high T_{CD8} PD-1 levels correlate with a positive clinical outcome, presumably due to reduced T_{CD8}-mediated liver damage (33). However, during acute hepatitis C virus infection, high PD-1 expression is associated with T_{CD8} impairment and progression to chronic infection (34). More recent studies have suggested that PD-1 plays an inhibitory role during some acute infections, such as viral central nervous system infection (35, 36), pulmonary fungal infection (37), and bacterial sepsis (38, 39). However, mechanisms governing PD-1 regulation in these settings and the specific impact of PD-1 signaling on T_{CD8} functional impairment during acute viral infections are unknown.

We hypothesized that viruses causing acute LRI induce PD-1–mediated T_{CD8} functional impairment in the infected lung, where both viral antigen driving PD-1 upregulation and PD-L1 ligating PD-1 are present. We report that PD-1 signaling rapidly induced pulmonary T_{CD8} impairment during HMPV and IAV infections. Using i.n. delivery of peptide-loaded DCs to elicit a T_{CD8} response in the absence of viral replication, we demonstrate that cognate viral antigen is necessary and sufficient to induce PD-1 upregulation, but that infection-induced PD-L1 is also required for T_{CD8} impairment. Importantly, therapeutic inhibition of PD-1

Conflict of interest: John V. Williams serves on the Scientific Advisory Board of Quidel.
Citation for this article: *J Clin Invest.* 2012;122(8):2967–2982. doi:10.1172/JCI62860.

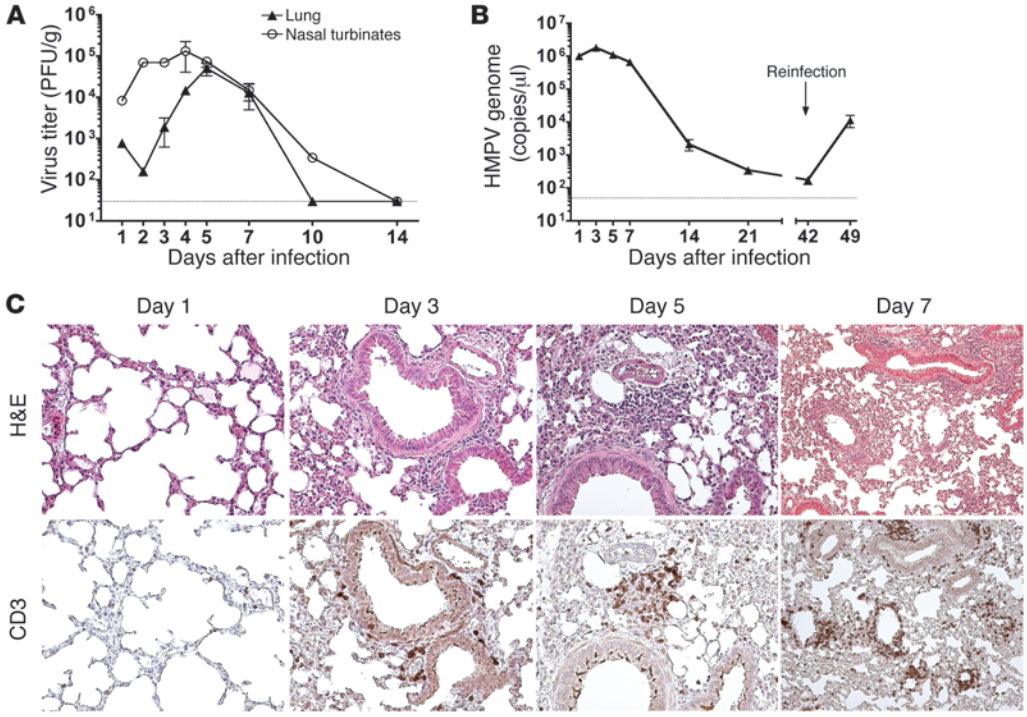

Figure 1
Kinetics of HMPV viral replication and lower airway pathology. (**A**) B6 mice were infected i.n. with HMPV and viral titers were quantified for the lungs and nasal turbinates in PFU per gram tissue (n = 3–6 mice per time point). Dotted line indicates the limit of viral detection. (**B**) Real-time RT-PCR targeting the HMPV N gene was used to quantify genome levels in the lungs of infected mice at the indicated times after infection (n = 5–10 mice per time point). Arrow indicates the time at which mice were challenged with HMPV. (**C**) Images represent serially cut lung sections stained with H&E or anti-CD3 and are representative of 3–5 individual mice per time point for which viral titers were determined to confirm infection. Original magnification, ×200 (days 1–5); ×100 (day 7). Data in **B** are representative of 3 experiments.

ligation using monoclonal antibody blockade prevented impairment and reduced viral titers without exacerbating lung histopathology, though mild airway dysfunction was observed. T_{CD8} impairment was more pronounced during secondary infection, as memory T_{CD8} were severely impaired and expressed more PD-1 than T_{CD8} during primary infection. PD-1 signaling blockade during challenge infection of immunized mice restored function to pulmonary T_{CD8} and significantly augmented their protective capacity, resulting in reduced viral titers. Finally, PD-1 and PD-L1 were expressed in the lungs of patients with severe acute viral LRI, suggesting that modulation of the PD-1/PD-L1 pathway could enhance antiviral T_{CD8} functions in these patients, a population for which limited treatment options currently exist.

Results

*HMPV T_{CD8} epitope mapping in C57BL/6 and HLA-B*0702 transgenic mice*. Since previous studies of HMPV disease in small animals utilized BALB/c mice (40, 41) or cotton rats (42), we first characterized HMPV infection of C57BL/6 (B6) mice. Viral titers peaked in the lungs at day 5 after infection, declined at day 7, and were undetectable by day 10 (Figure 1A), consistent with an acute infection (2). Viral genome was still detectable in the lungs up to 6 weeks after infection (Figure 1B). Lower airway histopathology was consistent with peribronchiolitis and perivasculitis (Figure 1C).

To more specifically study the anti-HMPV T_{CD8} response, we mapped epitopes in B6 mice as well as B6-Kb^0Db^0;B7.2 transgenic (B7tg) mice, which can only recognize T_{CD8} epitopes restricted by human HLA-B**0702* (43). In B6 mice, 11 epitopes were identified with similar frequencies of IFN-γ–secreting HMPV-immune splenocytes at day 10 after infection (data not shown and Supplemental Figure 1A; supplemental material available online with this article; doi:10.1172/JCI62860DS1). To determine which epitope-specific T_{CD8} targeted the primary site of HMPV infection, we further screened B6 epitopes in lung lymphocytes and determined that H2-D^b/$F_{528–536}$ (F528) and H2-K^b/$N_{11–19}$ (N11) resulted in the highest responses (Supplemental Figure 1A). In B7tg mice, 6 T_{CD8} epitopes were identified (Supplemental Figure 1B and data not shown). Stimulation with $M_{195–203}$ (M195) and to a lesser extent $N_{198–206}$ (N198) peptides produced a large fraction of HMPV-immune splenocytes releasing IFN-γ at day 10 after infection (Supplemental Figure 1B). HMPV replication kinetics and lung pathology in B7tg mice were similar to those in B6 mice (data not shown).

Pulmonary T_{CD8} are impaired and upregulate PD-1 during HMPV infection. HMPV-specific T_{CD8} were quantified using two separate assays performed in parallel: MHC class I tetramer staining enumerates total epitope-specific T_{CD8} directly ex vivo, while epitope restimulation followed by intracellular cytokine staining (ICS) for IFN-γ, a direct correlate of cytolytic activity (44), and surface staining for CD107a, an indicator of cytotoxic granule release (45), quantifies effector functions (Supplemental Figure 2 shows flow cytometry gating strategies). In the spleen, we observed a high concordance between tetramer staining and CD107a mobi-

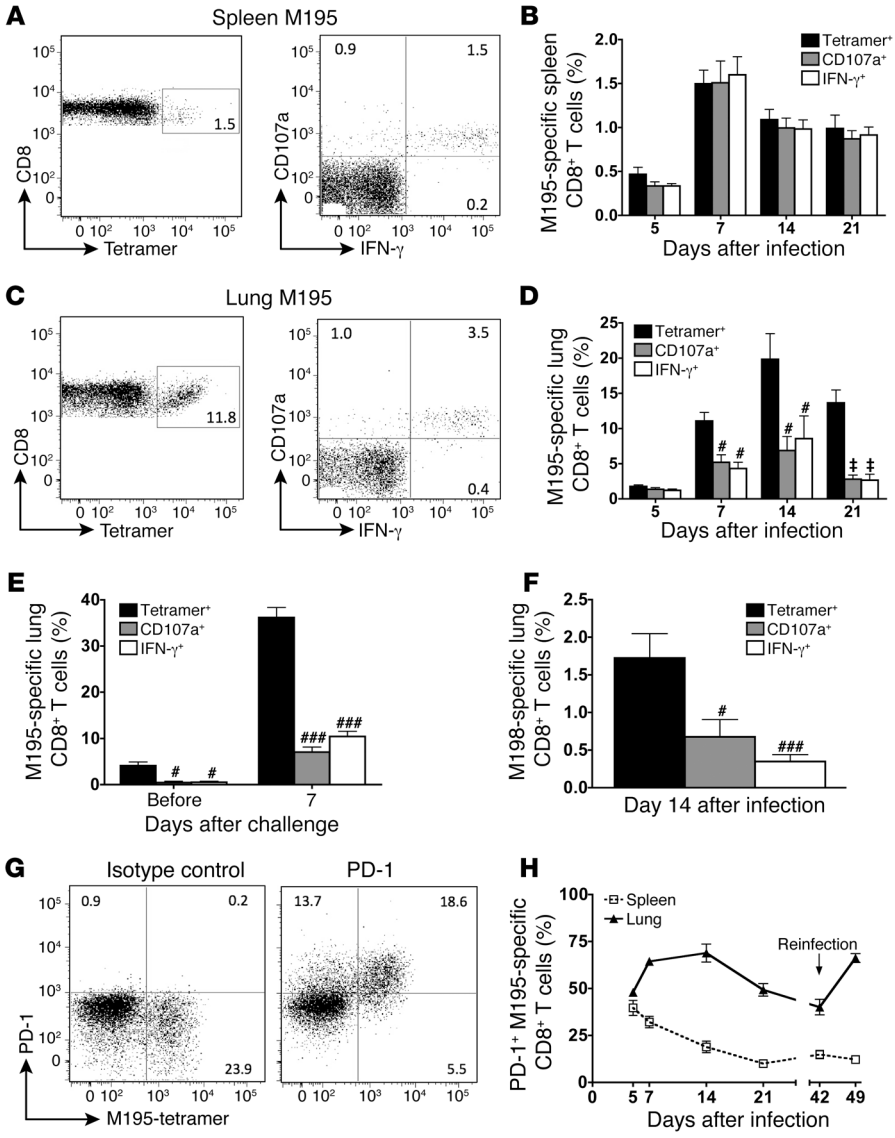

Figure 2

Pulmonary T_{CD8} are impaired and upregulate PD-1 during HMPV LRI. Spleen (**A** and **B**) and lung (**C** and **D**) lymphocytes were isolated from B7tg mice at the indicated times after HMPV infection. Representative histograms from day 7 after infection (**A** and **C**) and combined data from several time points (**B** and **D**) enumerate the T_{CD8} response directed against the M195 epitope. Numbers in flow plots indicate the percentage of CD8+ T cells that either bind to M195 tetramer or respond to restimulation with M195 peptide by mobilizing CD107a to the cell surface (i.e., degranulating) or producing IFN-γ. (**E**) M195-specific T_{CD8} response at day 42 after primary infection (Before) and then at day 7 after challenge. (**F**) N198-specific T_{CD8} response at day 14 after infection. (**G**) Representative flow cytometry plots demonstrating PD-1 expression versus M195 tetramer staining at day 14 after infection in the lung. Numbers in each quadrant indicate the percentage of CD8+ T cells. (**H**) Kinetics of PD-1 expression on spleen or lung M195-specific CD8+ T cells. Arrow indicates the time at which mice were challenged with HMPV (day 42 after primary infection). Data are representative of at least 2 independent experiments with 4–5 individual mice per time point. Twenty-thousand CD8+ T cells were counted for the spleen and 10,000 for the lung. $^{\#}P < 0.05$, $^{\ddagger}P < 0.005$, $^{\#\#\#}P < 0.0005$ (2-tailed paired *t* test); values in **D**–**F** are relative to tetramer+ cells analyzed in parallel from the same mice at the same time point.

lization or IFN-γ production in T_{CD8} at all time points (Figure 2, A and B). However, by day 7 after infection, 11.8% of lung-infiltrating T_{CD8} were detected with M195 tetramer, while only 3.5% produced IFN-γ or degranulated when restimulated with M195 peptide (Figure 2, C and D). Pulmonary T_{CD8} function continued to decline over time, with less than 10% functional by week 6 (Figure 2, D and E). Thus, a large fraction of pulmonary HMPV-specific T_{CD8} failed to respond to antigen, and this impairment persisted for several weeks beyond viral clearance.

During chronic infections or cancer, T_{CD8} become exhausted with progressive loss of effector functions; these cells lose expression of IL-2, TNF-α , IFN-γ , and CD107a, in that order, followed by clonal deletion (17). To define the extent of impairment during HMPV infection, we quantified other effector functions at the peak of the T_{CD8} response. Thirty-six percent of lung-infiltrating T_{CD8} expressed granzyme B (GzmB), which were predominantly M195 tetramer+ (Supplemental Figure 3A). While about two-thirds of M195-specific T_{CD8} were GzmB+, far fewer produced IFN-γ, and even fewer produced TNF-α or IL-2 (Supplemental Figure 3, B and C). Strikingly, lung M195-specific T_{CD8} were more severely impaired during secondary infection, when neutralizing antibody completely blocks viral replication in the lungs (Figure 2E and data not shown). Since M195 epitope–specific cells account for such a high percentage of virus-activated lung T_{CD8} during primary and secondary infection, we questioned whether T_{CD8} impairment was restricted to the immunodominant response. This was not the case, as subdominant N198-specific T_{CD8} were functionally impaired to a similar degree (Figure 2F), as were other epitopes tested (data not shown). Thus, pulmonary HMPV-specific T_{CD8} were impaired in multiple key effector functions.

Given the progressive degree of functional impairment observed in pulmonary HMPV-specific T_{CD8}, we wondered whether these cells expressed the inhibitory receptor PD-1, a marker of impaired T cells. In naive mice, less than 5% of lung or spleen T_{CD8} expressed PD-1 (data not shown). In contrast, during HMPV infection PD-1 was rapidly upregulated on M195-specific T_{CD8} by day 5 and reached maximum expression in the lungs between days 7 and 14 (Figure 2, G and H). Over half of pulmonary T_{CD8} remained PD-1+

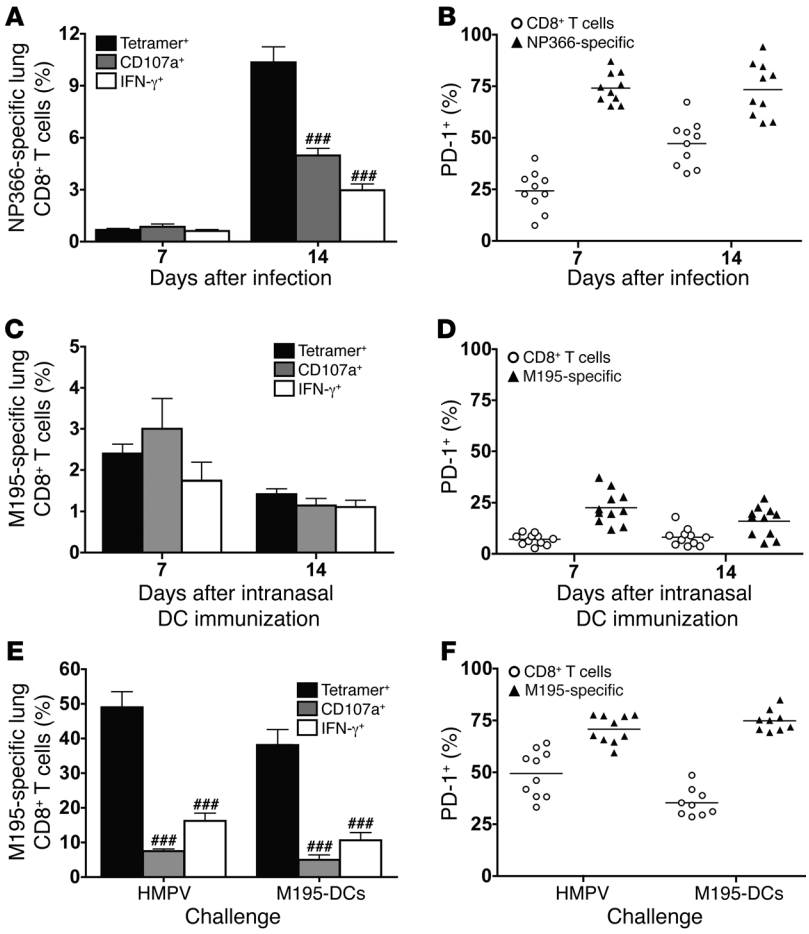

Figure 3
Viral infection is required for pulmonary T_{CD8} impairment and PD-1 upregulation. (**A** and **B**) B6 mice were infected with IAV (strain A/34/PR/8), and the lung T_{CD8} response (**A**) and PD-1 expression (**B**) were assessed at days 7 and 14 after infection for the H2-D^b/NP366 epitope. (**C** and **D**) B7tg mice were immunized i.n. with M195 peptide-loaded, LPS-matured DCs, and the lung M195-specific T_{CD8} response (**C**) and PD-1 expression (**D**) were quantified. (**E** and **F**) B7tg mice were infected with HMPV and then challenged at least 50 days later with either virus (HMPV) or M195-DCs delivered i.n. Lung lymphocytes were harvested at day 7 after challenge, and the T_{CD8} response (**E**) and PD-1 expression (**F**) were quantified. PD-1 expression on total lung $CD8^+$ lymphocytes and epitope-specific $CD8^+$ T cells are shown (**B**, **D**, and **F**). Each symbol represents an individual mouse, while horizontal lines denote the mean for each group. Data are combined from 2 independent experiments with 5 individual mice per time point per experiment. $^{###}P < 0.0005$ (2-tailed paired *t* test).

several weeks after viral clearance. Upon reinfection, PD-1 levels returned to those observed during primary infection (Figure 2H), despite undetectable lung virus replication (data not shown). In contrast, M195-specific T_{CD8} in the uninfected spleen upregulated PD-1 early during infection but steadily decreased expression over time, which did not increase upon challenge infection. PD-1 expression was not restricted to a limited TCR repertoire, as the M195-specific population was polyclonal, primarily representing the Vβ2 and Vβ9 families (Supplemental Figure 4A). PD-1 expression was indistinguishable between different TCR Vβ families (Supplemental Figure 4B) and different epitopes (Supplemental Figure 4C). Thus, prolonged PD-1 expression by a polyclonal lung T_{CD8} population was associated with impairment.

Viral infection is required for pulmonary T_{CD8} impairment and PD-1 upregulation. To determine whether T_{CD8} upregulate PD-1 in response to other acute viral LRIs, we infected B6 mice with influenza virus (strain A/34/PR/8) and measured lung T_{CD8} responses to the immunodominant H2-D^b/$NP_{366–374}$ (NP366) epitope (ref. 46 and Figure 3A). As previously described (8), we observed no impairment at day 7 after infection. However, there was substantial impairment of both IFN-γ production and degranulation by day 14, with the majority of pulmonary NP366-specific T_{CD8} expressing PD-1 at both time points (Figure 3B). Intranasal infection of B7tg mice with vaccinia virus (VACV) also resulted in T_{CD8} impairment and PD-1 upregulation for the immunodominant epitopes A34$R_{82–90}$ (A34R) and D1$R_{808–817}$ (data not shown). These data indicate that functional impairment of pulmonary PD-1^{hi} T_{CD8} is a common host response to different virus families capable of causing acute LRI.

Since several human viruses are capable of eliciting pulmonary T_{CD8} impairment, we wondered whether this was a consequence of T_{CD8} trafficking to the unique lung microenvironment. To address this, we employed peptide-loaded, LPS-matured bone marrow–derived DCs, which are potent antigen-presenting cells that, once administered, traffic to draining LNs to prime naive T_{CD8} (47, 48). Matured DCs were $CD11b^+$ and upregulated MHC molecules, costimulatory CD86, and the LN homing receptor CCR7 (Supplemental Figure 5A). DCs were loaded with M195 peptide and administered i.n. to recapitulate the route of infection utilized by respiratory viruses and to elicit epitope-specific T_{CD8} in the absence of viral replication. M195-specific T_{CD8} were detectable in the lung by day 5 after immunization (Supplemental Figure 5B), the same time HMPV-specific T_{CD8} arrived in the lung following HMPV infection (Figure 2B). Interestingly, lung-infiltrating M195-specific T_{CD8} elicited by DCs were not impaired at either day 7 or 14 after immunization (Figure 3C) and expressed low levels of PD-1 (~25%, Figure 3D) as compared with the level during HMPV infection (~75%, Figure 2H). Furthermore, DC-elicited M195-specific T_{CD8} were polyfunctional, with most containing GzmB and producing TNF-α and IL-2 in addition to IFN-γ (Supplemental Figure 5C). Next, mice were DC immunized either s.c. or i.n. to determine whether DC-elicited T_{CD8} provide protection against subsequent

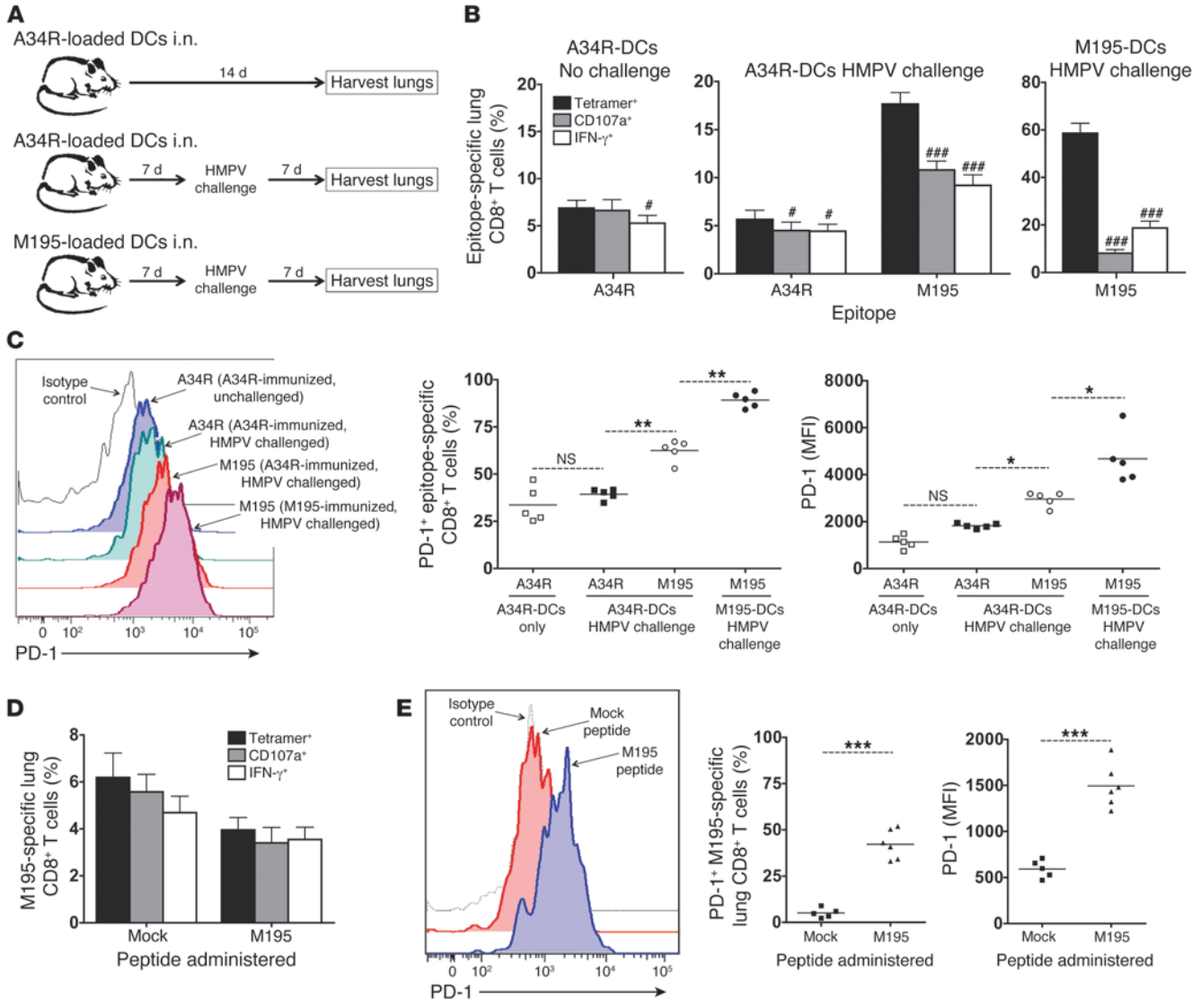

Figure 4

Cognate viral antigen in the presence of active LRI is required for PD-1 induction and T_{CD8} impairment. (**A**) Experimental strategy for **B** and **C**: B7tg mice were immunized i.n. with VACV A34R-loaded or HMPV M195-loaded DCs, and lung lymphocytes were harvested at either day 14 after immunization (A34R immunization) or day 7 after HMPV challenge (both A34R and M195 immunizations). (**B**) The A34R- and M195-specific T_{CD8} responses were quantified in each group of mice as indicated. (**C**) PD-1 expression is shown as either representative histograms, percentage positive, or MFI. (**D** and **E**) Mice were immunized i.n. with M195-loaded DCs, and then 50 μg of either an irrelevant peptide (Mock) or M195 peptide (M195) was administered daily i.n. for 7 days. The M195-specific T_{CD8} response (**D**) and PD-1 expression (**E**) following repeated peptide administration were quantified. Data in **B** are combined from 3 independent experiments, while data in **C**–**E** are representative of at least 2 independent experiments with 4–6 individual mice per group per experiment. $^{\#}P < 0.05$, $^{\#\#\#}P < 0.0005$ (2-tailed paired t test). $^{*}P < 0.05$, $^{**}P < 0.005$, $^{***}P < 0.0005$ (1-way ANOVA with Bonferroni post-test [**C**] or 2-tailed Student's *t* test [**E**]).

challenge infection. Following challenge of s.c. immunized mice, only M195-DCs decreased lung viral titers at the peak of virus replication (Supplemental Figure 5D). In contrast, i.n. immunization with DCs loaded with a VACV epitope (mock-DCs) or N198-DCs resulted in an 8- to 10-fold reduction in viral titers (Supplemental Figure 5E), suggesting that either residual DCs present in the lung or nonspecific pulmonary T_{CD8} provide some degree of protection. Importantly, i.n. immunization with M195-DCs resulted in an even greater, 35-fold reduction in viral titers as compared with unimmunized mice. Interestingly, mice infected with HMPV and then challenged i.n. with M195-DCs several weeks later exhibited the same degree of T_{CD8} impairment (Figure 3E) and PD-1 upregulation (Figure 3F) as mice undergoing secondary viral infection, suggesting that the impairment program is maintained in antigen-experienced peripheral memory T_{CD8}, a population that accounts for much of the recall response to secondary viral LRI (49).

Cognate viral antigen in the presence of active LRI is required for PD-1 induction and T_{CD8} impairment. Antigen-dependent TCR signaling is associated with PD-1 upregulation during chronic infections (18–20, 29), but a variety of cytokines can also induce PD-1 inde-

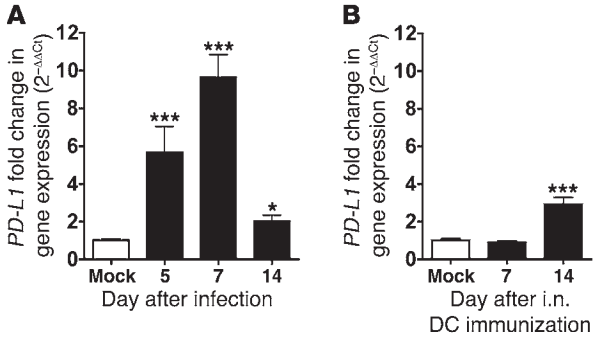

Figure 5
PD-L1 expression increases in lungs upon viral infection but not DC immunization. B7tg mice were either infected with HMPV (**A**) or immunized i.n. with M195-loaded DCs (**B**). At the indicated times after inoculation lung RNA was extracted for quantification of *PD-L1* gene expression using real-time RT-PCR. *PD-L1* levels were normalized to the housekeeping gene *Hprt*, and the relative gene expression compared with that in mock-infected animals is shown ($2^{-\Delta\Delta Ct}$ method). Data are combined from 2 independent experiments with 4–6 individual mice per time point per experiment. $^*P < 0.05$, $^{***}P < 0.0005$ compared with mock-infected mice (2-tailed Student's *t* test).

pendent of antigen exposure (50, 51). To determine whether viral antigen present at the site of infection is the primary cause of both pulmonary T_{CD8} impairment and PD-1 upregulation, we took advantage of the fact that i.n. DC immunization elicits unimpaired, PD-1^{lo} T_{CD8} directly in the lung environment (Figure 3, C and D). Therefore, we DC-immunized mice i.n. with either the VACV epitope A34R or the HMPV epitope M195. There is no cross-reactivity between A34R and any HMPV epitopes, as A34R tetramer failed to stain HMPV-immune splenocytes or lung lymphocytes (Supplemental Figure 2). A34R-immunized mice were either unchallenged or HMPV challenged, while M195-immunized mice were HMPV challenged (Figure 4A). A34R-specific T_{CD8} in unchallenged mice were not impaired (Figure 4B), as was the case with M195-specific T_{CD8} following M195-DC immunization (Figure 3C). Importantly, during HMPV challenge, A34R-specific T_{CD8} were not substantially impaired for either degranulation (Figure 4B and Supplemental Figure 6A) or IFN-γ production (Figure 4B and Supplemental Figure 6B), while M195-specific T_{CD8} in the same infected lungs were severely impaired as during primary infection. Thus, HMPV infection does not impair the functionality of heterologous VACV-specific T_{CD8}. M195-immunized HMPV-challenged mice mounted a robust secondary response to the M195 epitope, but their T_{CD8} were the most severely impaired (Figure 4B and Supplemental Figure 6, A and B), suggesting that antigen-experienced T_{CD8} are more susceptible to functional exhaustion than T_{CD8} responding to primary infection. The degree of impairment in each group correlated with PD-1 levels: PD-1 expression on A34R-specific T_{CD8} was similarly low in unchallenged and challenged mice (Figure 4C). In M195-immunized HMPV-challenged mice, almost 100% of M195-specific T_{CD8} were PD-1^+ (Figure 4C), and there was a 60% increase in MFI over that of M195-specific T_{CD8} in A34R-immunized mice (Figure 4C), indicating that PD-1 is more highly expressed during secondary immune responses.

During chronic infections, persistent viral antigen causes PD-1–mediated T_{CD8} exhaustion through continuous stimulation of the TCR (17, 18, 51, 52). To determine whether antigen exposure alone is capable of inducing PD-1 expression and functional impairment in the respiratory tract, we immunized mice i.n. with M195-loaded DCs and then administered either an irrelevant peptide or M195 peptide i.n. to provide cognate antigen for TCR stimulation. After reexposure to cognate antigen, M195-specific T_{CD8} remained fully functional (Figure 4D) but significantly upregulated PD-1 (Figure 4E), indicating that antigen-dependent TCR signaling is sufficient for PD-1 upregulation but not functional impairment in the acute setting.

Taken together, the preceding data suggested that both cognate viral antigen and active LRI are required for PD-1 induction and T_{CD8} impairment. Since cognate antigen alone failed to induce impairment in the absence of infection, we hypothesized that upregulation of the PD-1 ligand PD-L1 was also required. HMPV or IAV infection of human bronchial epithelial cells upregulated PD-L1 in a dose-dependent manner (Supplemental Figure 7), consistent with previous findings for RSV (27). HMPV also induced PD-L1 upregulation in the lungs of infected mice: *PD-L1* gene expression increased 4-fold by day 5 after infection and 10-fold by day 7, and decreased rapidly by day 14 (Figure 5A). In contrast, PD-L1 expression was unchanged on day 7 after DC immunization and increased slightly by day 14 (Figure 5B). Thus, PD-L1 expression increased early during viral infection in association with PD-1^{hi} T_{CD8}, but not during DC immunization, when T_{CD8} are PD-1^{lo}.

Blockade or ablation of PD-1 signaling prevents pulmonary T_{CD8} functional impairment during acute viral LRI. To prevent PD-1 ligation and determine whether pulmonary T_{CD8} impairment requires infection-induced PD-L1, we injected mice with blocking antibodies against PD-1 ligands (anti–PD-L) prior to infection and then every 2 days following infection. Anti–PD-L resulted in a greater percentage of M195-specific T_{CD8} in the spleens of infected animals, but more importantly improved function of pulmonary T_{CD8} compared with that in mice treated with isotype control antibody (Figure 6A). The percentage of functional M195-specific cells increased from 65% to 95% CD107a$^+$ and from 45% to 71% IFN-γ$^+$ in anti–PD-L mice compared with control mice (Figure 6B). Anti–PD-L also augmented the amount of IFN-γ synthesized in spleen and lung M195-specific T_{CD8} (Figure 6C). The percentage of PD-1^+ M195-specific T_{CD8} increased in both the spleen and lung of anti–PD-L–treated mice (Figure 6D), again indicating that PD-1 upregulation alone is insufficient to induce T_{CD8} impairment and that ligation by PD-L1 is also required. To gauge the broader immunomodulatory effects of blocking PD-1 signaling, we quantified total cytokine levels in HMPV-infected lungs. Anti–PD-L resulted in increased levels of the proinflammatory cytokines IFN-γ, TNF-α, and IL-6, while IL-17A and the anti-inflammatory cytokines IL-10 and TGF-β were unchanged (Figure 6E). Both IL-2 and IL-4 were below the limit of detection (data not shown). Importantly, prevention of pulmonary T_{CD8} impairment and augmentation of cytokine levels resulted in enhanced viral clearance, as anti–PD-L reduced lung viral titers 2-fold on day 5 after infection and more than 30-fold on day 7 (Figure 6F).

Despite the increased level of proinflammatory cytokines and functional T_{CD8}, anti–PD-L was not associated with increased lung histopathology (Supplemental Figure 8). However, to gauge more relevant clinical outcomes in live mice, we utilized a mouse oximeter to quantify airway dysfunction, a key feature of severe

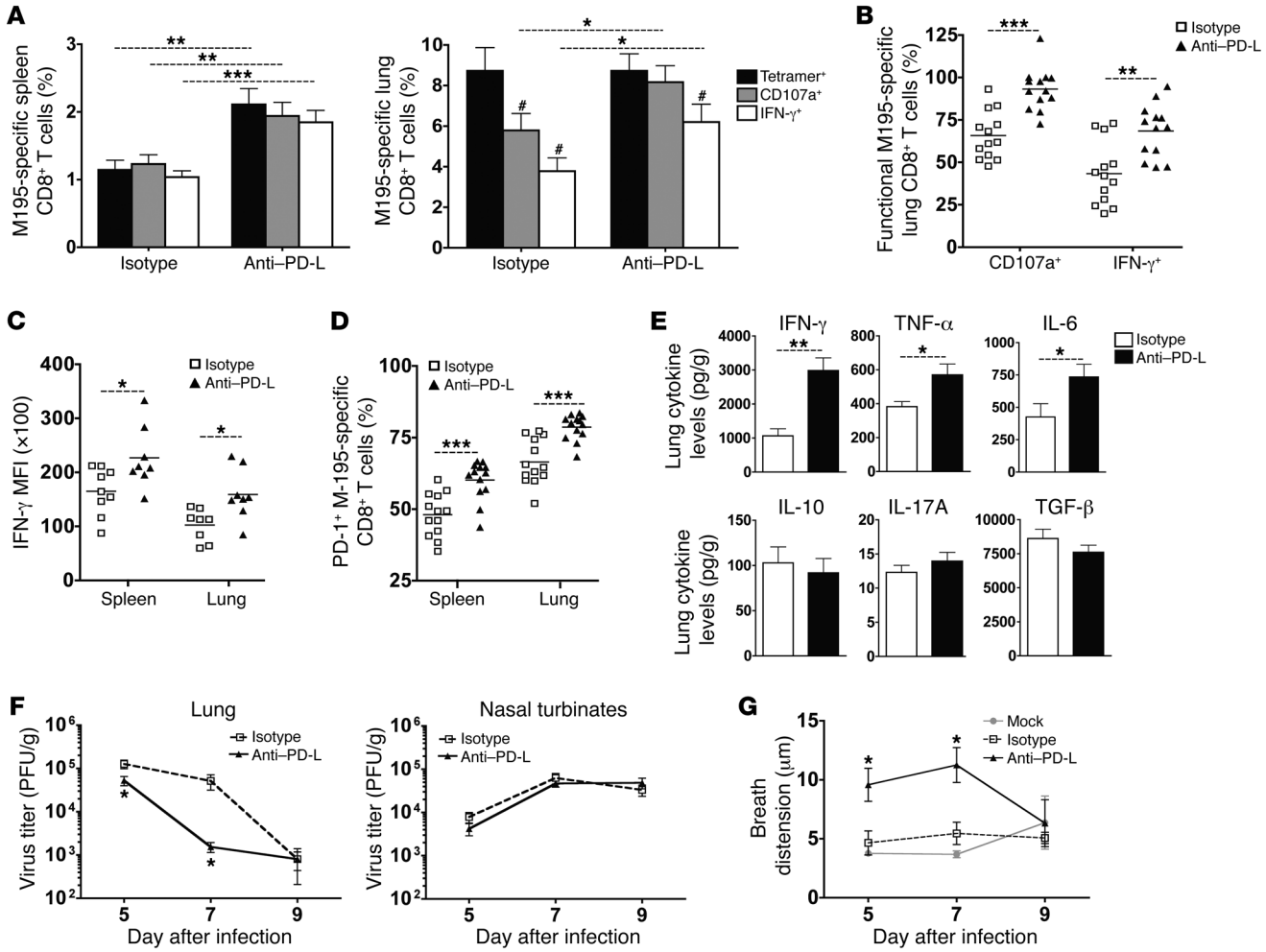

Figure 6

Blocking PD-1 ligation prevents functional impairment of pulmonary T_{CD8} during HMPV infection. B7tg mice were injected i.p. with 200 μg of isotype control antibody (Isotype) or both anti–PD-L1 and anti–PD-L2 blocking antibodies (Anti–PD-L) for 2 days prior to infection and then every other day during HMPV infection. (**A**) The M195-specific T_{CD8} response was quantified in the spleen and lung on day 7 after infection. (**B**) The percentage of functional M195-specific pulmonary T_{CD8} was calculated by dividing the percentage of $CD8^+$ T cells that were either $CD107a^+$ or IFN-γ^+ by the percentage of cells that were $tetramer^+$ for both isotype- and anti–PD-L–treated mice. (**C**) IFN-γ MFI from M195-stimulated cells. (**D**) PD-1 expression on spleen and lung M195-specific $CD8^+$ T cells. (**E**) Lung cytokines were quantified by cytometric bead array on day 7 after infection. (Note: IL-2 and IL-4 levels were below the limit of detection). (**F**) Lung and nasal turbinate viral titers were quantified via plaque assay on days 5, 7, and 9 after infection. (**G**) Breath distension of peripheral arteries, a measure of pulsus paradoxus and airway dysfunction, was quantified noninvasively by pulse oximetry as described in Methods. "Mock" indicates mice that were mock infected. Data in **A**–**E** are combined from 2 or 3 independent experiments with 4–5 individual mice per group per experiment, while data in **F** and **G** are representative of 2 independent experiments with 5 mice per group. $^{\#}P < 0.05$ (2-tailed paired *t* test); $^{*}P < 0.05$, $^{**}P < 0.005$, $^{***}P < 0.0005$ (2-tailed Student's *t* test).

LRI in humans (53). Airway dysfunction and subsequent air trapping leads to pulsus paradoxus, an exaggeration in the pulse volume during respiration as a result of increased breathing effort (54). HMPV infection alone did not increase breathing effort as compared with mock infection (Figure 6G). However, anti–PD-L resulted in double the breathing effort relative to that observed in isotype control–treated animals. Thus, anti–PD-L reduced functional impairment in a population of protective HMPV-specific T_{CD8}, but did, to some degree, increase airway dysfunction.

We next employed *PD-1*$^{-/-}$ mice (55) to completely abolish PD-1 signaling and confirm that results from anti–PD-L treatment were due to inhibition of PD-1 signaling and not reverse signaling through PD-L1 (51). *PD-1*$^{-/-}$ mice were maintained on the B6 background, so we examined the HMPV-specific T_{CD8} response directed against the F528 and N11 epitopes. Similar to mice treated with anti–PD-L, *PD-1*$^{-/-}$ mice had a higher percentage of splenic HMPV-specific T_{CD8} (Figure 7A), as well as a greater percentage of lung F528- and N11-specific T_{CD8} that degranulated and produced IFN-γ as compared with WT mice (Figure 7B). This translated to a greater percentage of functional pulmonary HMPV-specific T_{CD8} in *PD-1*$^{-/-}$ mice (Figure 7C). Unlike in the experiments with anti–PD-L, we also observed a 3- to 4-fold increase in the absolute number of both $tetramer^+$ (Figure 7D) and IFN-γ^+ (Figure 7E) T_{CD8} in *PD-1*$^{-/-}$ mice relative to WT mice (Figure 7E). IFN-γ and

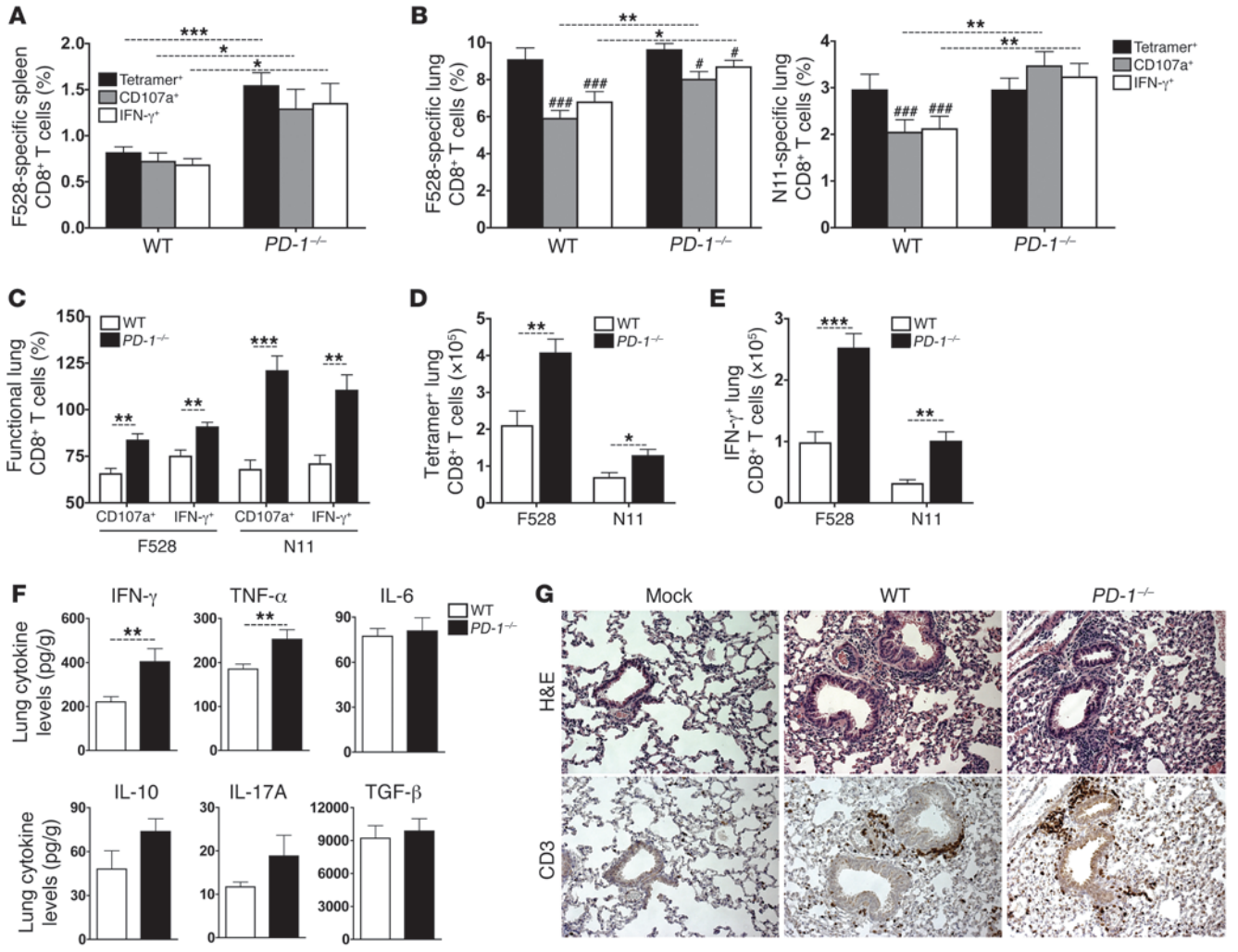

Figure 7

Pulmonary T_{CD8} impairment is prevented during HMPV LRI in *PD-1*$^{-/-}$ mice. WT and *PD-1*$^{-/-}$ mice were infected with HMPV, and 7 days later spleen and lung lymphocytes were harvested. (**A** and **B**) The spleen H2-D^b/F528–specific T_{CD8} response (**A**) and the lung F528 and H2-K^b/N11–specific T_{CD8} responses (**B**) were quantified. (**C**–**E**) The percentage of functional F528- or N11-specific lung T_{CD8} (**C**) as well as the absolute number of tetramer$^+$ (**D**) and IFN-γ$^+$ (**E**) epitope-specific cells was calculated. (**F**) Lung cytokines were quantified by cytometric bead array at day 7 after infection. (Note: IL-2 and IL-4 levels were below the limit of detection). (**G**) Lung sections from WT or *PD-1*$^{-/-}$ mice were either H&E or anti-CD3 stained. Images are representative of 4 individual mice per group. Original magnification, ×200. Data are combined from 2 (**F**) or 3 (**A**–**E**) independent experiments with 4–6 individual mice per group per experiment. $^{\#}P < 0.05$, $^{\#\#\#}P < 0.0005$ (2-tailed paired *t* test); $^{*}P < 0.05$, $^{**}P < 0.005$, $^{***}P < 0.0005$ (2-tailed Student's *t* test).

TNF-α cytokine levels were significantly elevated in the lungs of *PD-1*$^{-/-}$ animals, while IL-10 and IL-17A were trending upward and IL-6 and TGF-β were unchanged (Figure 7F). Given both the increased number of HMPV-specific T_{CD8} and their increased functionality in *PD-1*$^{-/-}$ mice, we asked whether PD-1 signaling functions to prevent immunopathology during acute viral LRI. WT and *PD-1*$^{-/-}$ mice exhibited the same pattern of peribronchiolitis and perivasculitis, with similar numbers of CD3$^+$ mononuclear cells infiltrating each of these spaces (Figure 7G), suggesting that abrogation of PD-1 signaling in the setting of acute LRI does not exacerbate lower airway histopathology.

We next tested the effect of PD-1 ablation on influenza virus LRI. Because T_{CD8} were not impaired on day 7 (Figure 3A), we examined the T_{CD8} response at day 8 after infection with IAV (strain HK/x31) in WT versus *PD-1*$^{-/-}$ mice. NP366-specific pulmonary T_{CD8} drastically upregulated PD-1 in WT mice (Figure 8A) and were impaired (Figure 8B). IFN-γ$^+$ and CD107a$^+$ NP366-specific T_{CD8} were increased in the lungs of *PD-1*$^{-/-}$ mice compared with WT animals (Figure 8, B and C). The IAV-specific *PD-1*$^{-/-}$ T_{CD8} did not contain more GzmB (Figure 8D), suggesting that increased supernatant GzmB levels found in some studies may be attributable to increased degranulation and not increased production (29, 56), while more prolonged blockade of the PD-1 pathway may be necessary to increase T_{CD8} granzyme expression (21, 57). *PD-1*$^{-/-}$ mice took longer to recover from infection than WT mice, as measured by weight loss (Figure 8E). Additionally, both WT and *PD-1*$^{-/-}$ animals exhibited increased breathing effort compared with mock-infected mice, but, in contrast to anti–PD-L treatment

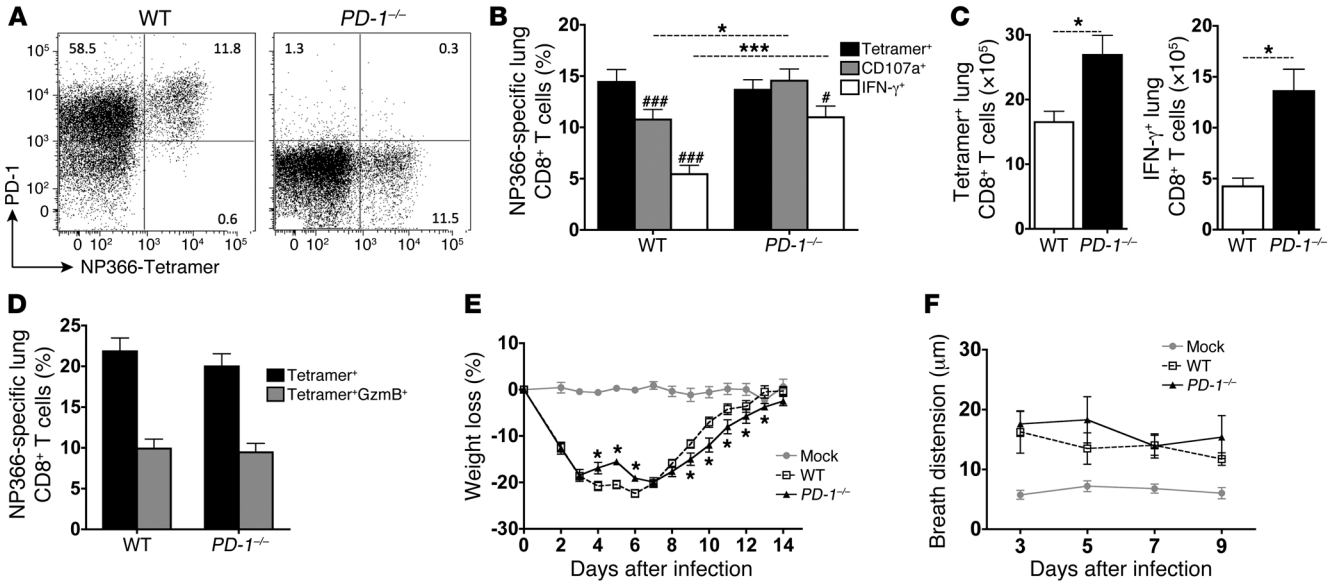

Figure 8

Pulmonary T_{CD8} impairment is improved but recovery is delayed in IAV-infected *PD-1*$^{-/-}$ mice. WT and *PD-1*$^{-/-}$ mice were infected with IAV (strain HK/x31), and 8 days later lung lymphocytes were isolated. (**A**) Representative flow cytometry plots showing PD-1 staining on NP366-specific T_{CD8} in WT versus *PD-1*$^{-/-}$ mice. Numbers in each quadrant indicate the percentage of CD8$^+$ T cells. (**B**) Quantification of the lung NP366-specific T_{CD8} response. (**C**) The absolute number of tetramer$^+$ or IFN-γ$^+$ NP366-specific lung T_{CD8} was calculated. (**D**) NP366 tetramer-labeled cells were permeabilized and stained for intracellular GzmB. (**E**) Weight loss is shown as a percentage of initial body weight. (**F**) Breath distension was measured as described in Methods. "Mock" indicates mice that were mock infected. Data are combined from 2 (**F**) or 3 (**A**–**E**) independent experiment with 5 individual mice per group per experiment. $^{\#}P < 0.05$, $^{\#\#\#}P < 0.0005$ (2-tailed paired *t* test); $^{*}P < 0.05$, $^{***}P < 0.0005$ (2-tailed Student's *t* test).

of HMPV-infected mice, lack of PD-1 signaling did not exacerbate airway dysfunction (Figure 8F). The results of these experiments suggest that PD-1 negatively regulates T_{CD8} during LRI caused by both HMPV and IAV, which may help to speed recovery by limiting adverse immune-mediated effects on respiratory physiology.

Anti–PD-L treatment improves secondary immune responses by overcoming T_{CD8} impairment during challenge infection. Given the large degree of impairment observed during secondary infection (Figure 2E and Figure 4B) or DC challenge of previously infected mice (Figure 3E), we sought to elucidate the role of PD-1 in inhibiting secondary immune responses. Since primary HMPV infection elicits sterilizing immunity, we employed i.n. DC immunization to elicit lung-infiltrating M195-specific T_{CD8} in the absence of infection. Mice were challenged with HMPV 18 days after immunization, and the M195-specific secondary immune response and viral titers were quantified at day 5 after challenge in either the presence or absence of anti–PD-L treatment (Figure 9A). Mice that were not DC immunized generated a small M195-specific response (1.3% tetramer$^+$, Figure 9B), consistent with previous results observed during primary infection (Figure 2D). Mice that were M195-DC immunized and isotype treated mounted a robust secondary M195-specific response (8% tetramer$^+$, Figure 9B). However, only half of these cells were functional as determined by CD107a mobilization (56%) and IFN-γ production (45%) (Figure 9, B and C). Anti–PD-L significantly restored both degranulation (87%) and IFN-γ production (81%) to M195-specific cells during challenge infection (Figure 9, B and C). Like anti–PD-L treatment during primary infection, blocking PD-1 ligation resulted in PD-1 upregulation on M195-specific T_{CD8} (Figure 9D). Importantly, lung viral titers in anti–PD-L–treated mice were reduced 5-fold compared with isotype-treated mice and more than 20-fold compared with unimmunized HMPV-infected mice (Figure 9E). Taken together, these results indicate that pulmonary T_{CD8} impairment during both primary and secondary infection is mediated by the PD-1/PD-L1 pathway and that this impairment can be prevented to maintain functional antiviral T_{CD8} and enhance viral clearance.

PD-1 and PD-L1 are expressed in the lower airways of patients with severe 2009 H1N1 pandemic IAV, RSV, or PIV-3 infection. To determine whether the PD-1/PD-L1 pathway is activated during acute viral LRI in humans, we obtained autopsy specimens from pediatric and adult patients with severe LRI or nonpulmonary disease as controls. Both 2009 H1N1 pandemic IAV and RSV caused pronounced lung pathology, including severe pneumonia (Figure 10B) and bronchiolitis (Figure 10C), with extensive T_{CD8} infiltration (Figure 10, F and G). PD-1 was detected on small lymphocytes and macrophages present in the airway and interstitium (Figure 10, J and K, and Supplemental Figure 9), while PD-L1 was expressed on alveolar and bronchiolar epithelial cells, as well as on airway and tissue macrophages (Figure 10, N, O, R, and S, and Supplemental Figure 9). In total, PD-1 was detected in 3 of 4 2009 H1N1 cases, 2 of 3 RSV cases and 1 of 1 PIV-3 case. PD-L1 was detected in 4 of 4 H1N1 cases, 3 of 3 RSV cases, and 1 of 1 PIV-3 case. In control cases (4 total), PD-1 and PD-L1 expression was restricted to sparse airway macrophages (Figure 10 and Supplemental Figure 9). These results suggest that the PD-1/PD-L1 pathway is engaged and may play a significant role in inhibiting adaptive immune responses during acute viral LRI in humans.

Discussion

Pulmonary T_{CD8} impairment has been described during murine acute viral LRI (8–12), but the mechanism has not been elucidated.

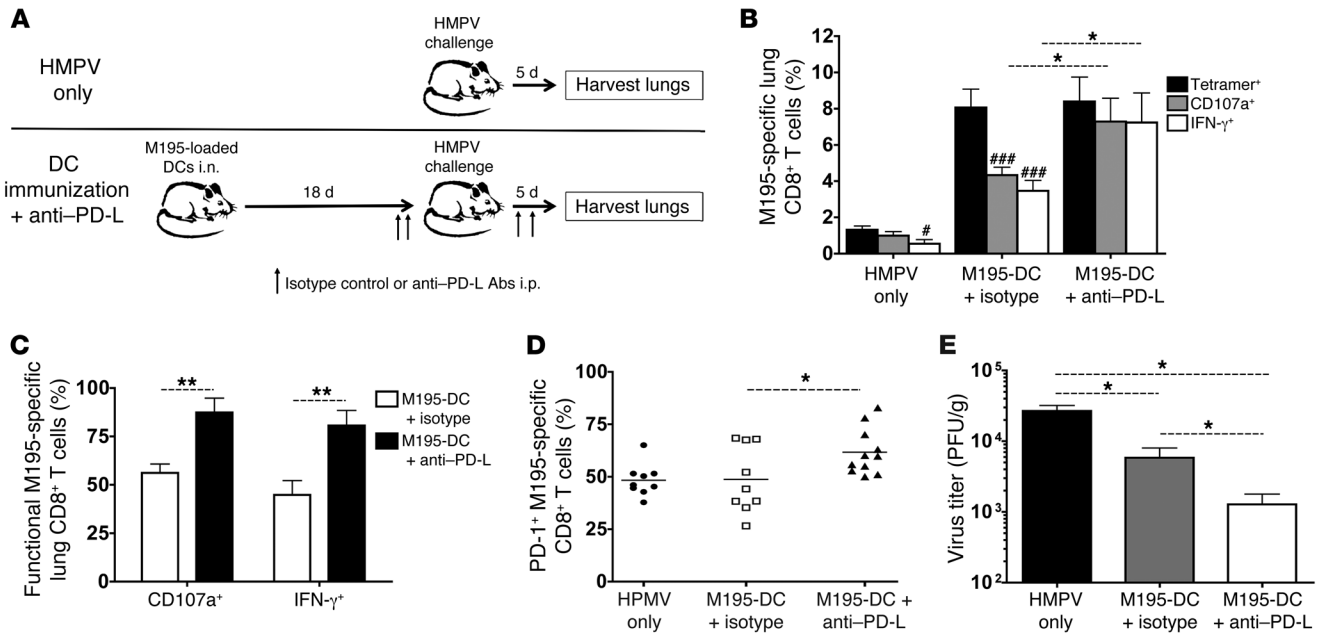

Figure 9

Anti–PD-L treatment improves secondary immune responses by overcoming T_{CD8} impairment during challenge infection. (**A**) Experimental strategy: mice were either not immunized (HMPV only) or immunized i.n. with M195-loaded DCs. Eighteen days later, mice were challenged with HMPV. Immunized mice were injected i.p. with isotype control antibody (M195-DC + isotype) or both anti–PD-L1 (250 μg) and anti–PD-L2 (200 μg) blocking antibodies (M195-DC + anti–PD-L) for 2 days prior to infection and then on days 1 and 3 during HMPV infection. (**B** and **C**) Five days after challenge, the lung M195-specific T_{CD8} response was quantified (**B**), and the functionality of these cells was calculated (**C**). (**D**) PD-1 expression of lung M195-specific T_{CD8}. (**E**) Lung viral titers were quantified by plaque assay. Data are combined from 2 independent experiments with 4–6 individual mice per group per experiment. $^{\#}P < 0.05$, $^{\#\#\#}P < 0.0005$ (2-tailed paired *t* test); $^{*}P < 0.05$, $^{**}P < 0.005$ (2-tailed Student's *t* test).

We show in two different mouse models and during both primary and secondary LRI that the PD-1/PD-L1 pathway mediates this impairment. Both dominant and subdominant epitope-specific T_{CD8} were impaired during HMPV, IAV, or VACV infection, indicating that loss of pulmonary T_{CD8} function via PD-1 signaling is not restricted to a single virus family. Pulmonary T_{CD8} impairment resembles the exhaustion phenotype observed during chronic viral infections, wherein T_{CD8} upregulate PD-1 and fail to respond when restimulated by viral antigen. T_{CD8} exhaustion occurs several weeks after infection, with the ability to produce IFN-γ and TNF-α lost first, followed by impairment of degranulation and cytotoxic capabilities (17, 19). In contrast, we found that PD-1–mediated pulmonary T_{CD8} impairment occurred rapidly (by day 7 after infection), with simultaneous loss of degranulation and IFN-γ production that continued for several weeks after viral clearance.

Since PD-1 was upregulated early during acute viral LRI on T_{CD8} but also maintained for several weeks following clearance, it is unclear whether early exposure to viral antigen or persistent low-level TCR stimulation from residual antigen maintains PD-1–mediated impairment after viral clearance. DC (Figure 3, C and D) and DNA immunization (8) experiments suggest that it may be the former, as T_{CD8} elicited in these antigen-low environments maintain effector capabilities. In the current study, we could not detect infectious virus in the lung past day 10; nonetheless, we did find trace amounts of viral genome via real-time RT-PCR up to 50 days after infection, similar to genome persistence described for both RSV (58) and IAV (59). This result suggests that persistent viral genome may provide a source of viral antigen to maintain TCR signaling and PD-1 expression even after infectious virus has been eliminated. Additionally, we found that splenic T_{CD8} were unimpaired and downregulated PD-1 over time, indicating that trafficking away from the infected lung and escape from antigen-driven TCR signaling may prevent impairment.

Additionally, cognate viral antigen in the context of active LRI was required for both pulmonary T_{CD8} impairment and PD-1 expression. Pulmonary T_{CD8} elicited by i.n. DC immunization, a context in which antigen is only transiently presented by the immunizing DCs before MHC class I internalization (60), were unimpaired and PD-1^{lo}. Additionally, heterologous VACV-specific T_{CD8} remained unimpaired and PD-1^{lo} even during HMPV challenge, indicating that antigen-dependent TCR signaling is the primary driver of impairment and PD-1 expression in this setting. However, antigen alone was not sufficient to induce impairment at early time points, as providing cognate peptide to M195-specific T_{CD8} in the lungs of M195-DC immunized mice upregulated PD-1 but did not cause impairment. It is possible that more long-term stimulation with antigen may eventually induce impairment. In one model system, chronic antigen stimulation achieved by repeated i.p. injections of IAV led to T_{CD8} exhaustion, as shown by a severe proliferation defect (61). However, impairment in this setting was not reversed by PD-L1 blockade and was more dependent on TRAIL signaling. During most LRIs both antigen and inflammation are abundantly present, so determining the precise role of each in mediating impairment represents a challenge. Our results would suggest that antigen-dependent TCR signaling is an important determinant of PD-1 expression, but that inflamma-

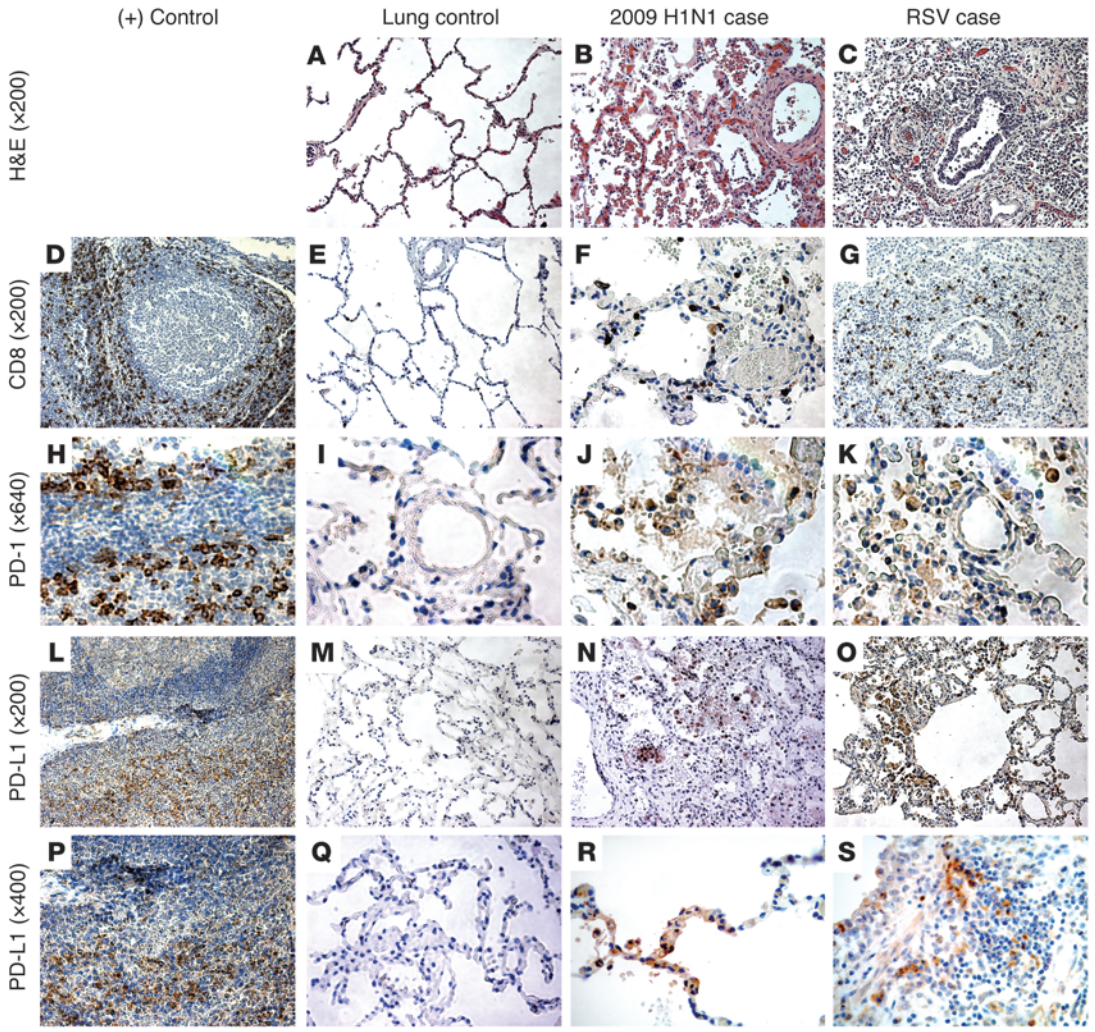

Figure 10
PD-1 and PD-L1 are expressed in the lower airways of pediatric patients with severe 2009 H1N1 pandemic IAV or RSV infection. Lung autopsy specimens were fixed and stained with H&E (**A**–**C**), anti-CD8 (**D**–**G**), anti–PD-1 (**H**–**K**), or anti–PD-L1 (**L**–**S**) antibodies. Tonsil (**D** and **H**) or spleen (**L** and **P**) tissue were used as positive controls. "Lung control" (**A**, **E**, **I**, **M**, and **Q**) is from a patient with non-pulmonary disease, while "2009 H1N1 case" (**B**, **F**, **J**, **N**, and **R**) is from a 12-year old patient with 2009 H1N1 pandemic IAV infection and "RSV case" (**C**, **G**, **K**, **O**, and **S**) is from an 18-month-old child with RSV infection. Original magnifications as indicated.

tion is also required for the induction of PD-1 ligands and subsequent inhibitory signaling.

Therefore, we hypothesized that regulation and expression of PD-L1 contributes significantly to impairment during acute viral LRI. In vitro, both HMPV and IAV infection of human bronchial epithelial cells resulted in PD-L1 upregulation, corroborating findings from studies with RSV, where it was also shown that IFN-γ alone is capable of increasing PD-L1 (27). In vivo, we found that PD-L1 expression correlated with viral replication and the induction of the adaptive immune response, as PD-L1 was upregulated 6-fold by day 5 after infection (the peak of viral replication) and 10-fold by day 7. HMPV, RSV, and IAV all infect respiratory tract epithelial cells. Antiviral T_{CD8} must recognize and interact with these infected cells in order to clear each virus. Furthermore, it has been demonstrated that RSV infection of primary human bronchial epithelial cells induced PD-L1 upregulation, leading to impairment of human T_{CD8} in vitro (56). Therefore, we propose a model whereby viral antigen signaling through the TCR leads to PD-1 upregulation on pulmonary T_{CD8}, while viral infection of airway epithelial cells induces PD-L1, leading to PD-1 ligation and inhibitory signaling when T_{CD8} interact with infected cells. This may represent a negative feedback loop designed to protect the lung against immune-mediated damage. Antiviral T_{CD8} enter the lung at day 5 after infection capable of degranulating and producing IFN-γ, yet by day 7 they show signs of impairment. IFN-γ produced by either $CD8^+$ or $CD4^+$ T cells may then upregulate PD-L1 on respiratory epithelial cells, thereby initiating PD-1 signaling in antiviral T_{CD8} and downregulating their effector functions. This contrasts with chronic viral infections caused by LCMV (62, 63) and HIV (63), where myeloid cells have been shown to contribute more to impairment and exhaustion, suggesting that viral tropism may dictate which cell types mediate impairment. In the case of

viral LRI, it could be infected lung epithelial cells, adjacent cells exposed to type I or type II IFNs, or both of these cell populations that contribute to T_{CD8} impairment in vivo.

We show that pulmonary T_{CD8} impairment is preventable, indicating a novel therapeutic avenue for acute viral LRIs, for which few specific treatments currently exist. Disruption of PD-1 signaling via therapeutic antibody blockade preserved T_{CD8} effector functions and decreased viral titers. As T_{CD8} functions also improved during both HMPV and IAV infections of *PD-1*$^{-/-}$ mice, targeting the PD-1/PD-L1 pathway may provide clinical utility by enhancing antiviral T_{CD8} during a variety of acute LRI. Increasing T_{CD8} effector functions and the presence of proinflammatory cytokines did not exacerbate airway histopathology in either anti–PD-L–treated or *PD-1*$^{-/-}$ mice. This contrasts with both chronic LCMV infection (19) and acute coronavirus CNS infection (35), where *PD-L1*$^{-/-}$ mice exhibited exacerbated pathology and increased mortality, indicating that PD-1 may play differential roles depending on the virus and site of infection. We observed differences even among LRI caused by different viruses, as anti–PD-L treatment of HMPV-infected mice resulted in mildly increased breathing effort and pulsus paradoxus, whereas IAV infected *PD-1*$^{-/-}$ mice displayed no enhanced airway dysfunction compared with WT mice. Thus, a therapeutic "window" for PD-1/PD-L1 modulation during acute viral LRI may exist between enhanced protection and immunopathology. Direct manipulation of the PD-1/PD-L1 pathway has so far proven safe and at least partially effective against both hematologic malignancies (30) and solid tumors (31) in humans and against SIV in nonhuman primates (57). Cytokine therapies that indirectly overcome PD-1 signaling also hold therapeutic promise (64, 65).

DC challenge of HMPV-primed mice was not capable of overcoming the impairment program set in motion during primary infection, adding to recent findings that high levels of viral antigen present during the initial infection mediate chromatin remodeling around the PD-1 locus, allowing for rapid expression in memory T_{CD8} upon reexposure to antigen (66). Furthermore, our results and those from the LCMV chronic infection model (67) indicate that antigen-experienced T_{CD8} are highly susceptible to PD-1–mediated impairment. During challenge infection, T_{CD8} rapidly upregulated PD-1 and were more severely impaired than during primary infection. Following DC immunization, we demonstrated that memory T_{CD8} provide some protection against viral challenge, which can be augmented by blocking PD-1 signaling. Therefore, modulation of the PD-1/PD-L1 pathway should be considered in the rational design of novel HMPV, RSV, or IAV vaccines. Future experiments are needed to further uncover the role of PD-1 in inhibiting memory T_{CD8} responses.

Finally, we determined that PD-1 and PD-L1 are abundantly expressed in the lower airways during acute viral LRI in humans. Additional studies are needed to determine whether PD-1 levels are associated with T_{CD8} impairment and poor clinical outcomes in patients with severe acute viral LRI. However, unlike in chronic infections with HIV and HCV, peripheral blood T_{CD8} may not exhibit functional impairment, and thus examination of pulmonary T_{CD8} will be required. Additionally, while our findings suggest that the PD-1/PD-L1 pathway may contribute to severe disease in humans, it will be interesting to determine what role this pathway plays in the ability of common respiratory viruses to continuously reinfect individuals. Human airway epithelial cells upregulate PD-L1 and PD-L2 in response to IFN-γ and TNF-α in vitro (27, 68) and to human rhinovirus infection in vivo (69). Therefore, upon reinfection, upper and lower respiratory tract epithelial cell PD-L would be poised to impair airway-resident memory T cells as well as newly recruited cells, thus preventing an effective early immune response to limit viral replication. Results from anti–PD-L–treated mice that were DC immunized suggest that memory T_{CD8} may be similarly, if not more, affected by PD-1 signaling than naive cells. Taken together, our results indicate that antigen-dependent PD-1 upregulation and subsequent ligation by PD-L1 play a prominent role in mediating pulmonary T_{CD8} impairment. These findings suggest that targeting the PD-1/PD-L1 pathway may provide therapeutic potential in patients with acute viral LRI and offer novel approaches for developing effective respiratory viral vaccines.

Methods

Mice and viruses

B6 mice were purchased from the Jackson Laboratory. B7tg mice were obtained with permission from Alexander Sette (La Jolla Institute for Allergy and Immunology, La Jolla, California, USA) and François Lemonnier (Institut Pasteur, Paris, France). *PD-1*$^{-/-}$ mice were obtained with permission from Tasuku Honjo (Kyoto University, Kyoto, Japan). All animals were bred and maintained in specific pathogen–free conditions in accordance with the Vanderbilt Institutional Animal Care and Use Committee. Six- to 12-week-old age- and sex-matched animals were used in all experiments. HMPV (pathogenic clinical strain TN/94-49, genotype A2) was grown and titered in LLC-MK2 cells as previously described (42). Influenza virus strains A/34/PR/8 (PR8; H1N1; ATCC) and HK/x31 (x31; H3N2; provided by Jon McCullers, St. Jude Children's Hospital, Memphis, Tennessee, USA) were grown in MDCK cells and titered on LLC-MK2 cells. The CR-19 strain of VACV was grown and titered on BSC-40 cells. For all experiments, mice were anesthetized with ketamine-xylazine and infected i.n. with 1.5×10^6 PFU of HMPV, 10^2 PFU of PR8, 5×10^2 PFU of x31, or 10^4 PFU of VACV in a 100-μl volume. x31 was used in experiments with *PD-1*$^{-/-}$ mice because it induced a more robust $CD8^+$ T cell response than PR8.

Viral titration and quantification of total lung cytokines

Viral titers were measured by plaque titration as previously described (42). Cytometric Bead Array was used to quantify IFN-γ, TNF-α, IL-2, IL-4, IL-6, IL-10, IL-17A, and TGF-β cytokine levels in undiluted lung homogenates according to the manufacturer's instructions (BD Biosciences).

Epitope prediction, synthetic peptides, and IFN-γ ELISPOT assays

The online prediction algorithms SYFPEITHI (http://www.syfpeithi.de/), BIMAS (http://www-bimas.cit.nih.gov/molbio/hla_bind/), and IEDB (http://www.immuneepitope.org/) were used to generate HMPV epitope predictions for the HLA-B**0702* (70), H2-D^b, and H2-K^b alleles. The top approximately 80 HLA-B**0702*–, 40 H2-D^b–, and 40 H2-K^b–restricted 8- to 10-amino-acid-long predictopes were synthesized for HLA-B**0702* (by Mimotopes) or $H2^b$ (by Genscript) to greater than 95% purity as determined by analytical high-performance liquid chromatography. ELISPOT analysis was performed as previously described (71). The mitogen concanavalin A (ConA, Sigma-Aldrich) was used as a positive control, while stimulation with an irrelevant peptide served as the negative control. The average number of spots in the negative control wells was subtracted from each experimental value, which was then expressed as spot-forming cells (SFC) per 10^6 lymphocytes.

Generation of MHC class I tetramers

The construct encoding a hybrid heavy chain of the HLA-B**0702* molecule was designed by replacing amino acids 206–299 of the human α3 domain

(NCBI RefSeq NM_002116.6 and NM_005514.6) with amino acids 203–296 from the mouse H2-K^b molecule (NCBI RefSeq NM_001001892.2). Constructs expressing H2-K^b and -D^b heavy chains were previously described (72). Recombinant heavy chains encoding a C-terminal BirA recognition sequence and β_2m were produced in *Escherichia coli* as described (73). MHC class I monomers were refolded with cognate conditional peptide ligands (74), biotinylated, and purified as described (75). UV-mediated exchange of conditional peptide with virus-derived peptides and quantification of peptide exchange were conducted as previously described (76). MHC tetramer formation with PE- and APC-streptavidin–conjugated fluorochromes (Invitrogen) was performed as previously described (76). Tetramers were generated for the following viral epitopes: HMPV (HLA-B*0702/M$_{195–203}$ [APYAGLIMI], HLA-B*0702/N$_{198–206}$ [YPRMDIPKI], H2-D^b/F$_{528–536}$ [SGVTNNGFI], H2-K^b/N$_{11–19}$ [LSYKHAIL]); influenza virus (H2-D^b/NP$_{366–374}$ [ASNENMETM]); and VACV (HLA-B*0702/A34R$_{82–90}$ [LPRPDTRHL], HLA-B*0702/D1R$_{808–817}$ [RPSTRNFFEL]).

Tetramer staining

Lymphocytes were isolated from spleens and lungs of infected animals as follows: lungs were rinsed in R10 medium (RPMI-1640 [Mediatech] plus 10% FBS, 2 mM glutamine, 50 μg/ml gentamicin, 2.5 μg/ml amphotericin B, and 50 μM β-mercaptoethanol [Gibco, Invitrogen]) to remove blood. The lungs were then minced with a scalpel and incubated with 2 mg/ml collagenase A (Roche) and 20 μg/ml DNase (Roche) for 1 hour at 37°C. Single-cell suspensions of digested lungs or whole spleens were obtained by pressing through a steel screen (80 mesh) and then passing over a nylon cell strainer (70-μm pore size). Erythrocytes were lysed using Red Blood Cell Lysis Buffer (Sigma-Aldrich). 2 × 10^6 to 3 × 10^6 lymphocytes were added to each well of a 96-well round-bottom plate (Falcon). Lymphocytes were first stained with violet LIVE/DEAD dye (Invitrogen) according to the manufacturer's instructions, then Fc blocked with 1 μg per 10^6 cells anti-CD16/32 (BD Biosciences), and finally incubated with PE- or APC-labeled tetramers (0.1–1 μg/ml), anti-CD8α (clone 53-6.7, BD Biosciences), and anti-CD19 (clone 1D3, eBioscience). In some experiments, cells were also stained for PD-1 (clone J43, BD Biosciences) or with an isotype control antibody (hamster IgG2κ). Surface/tetramer staining was performed for 1.5 hours at 4°C in PBS containing 1% FBS for HLA-B*0702 tetramers. For H2^b tetramers, surface/tetramer staining was performed for 1 hour at room temperature in FACS buffer containing 50 nM dasatinib (LC Laboratories) (77), as preliminary experiments demonstrated enhanced tetramer staining under these conditions. Background staining levels with an irrelevant tetramer (typically 0.05%–0.2% of CD8$^+$ T cells) were subtracted from each experimental value. For intracellular GzmB staining, cells were additionally surface stained for CD62L (clone MEL-14, BD Biosciences) and then fixed and permeabilized (BD Fix/Perm Reagent) and incubated with anti-GzmB (clone GB12, Invitrogen) for 30 minutes at 4°C. GzmB$^+$ cells were identified by exclusionary gating from the CD62L$^+$ population as previously described (78). Flow cytometric data were collected using an LSR II (BD Biosciences) and analyzed with FlowJo software (Tree Star).

Peptide restimulation and ICS

In parallel with tetramer staining, lung or spleen lymphocytes isolated from the same mice were restimulated in vitro for 6 hours at 37°C with the indicated synthetic peptide (10 μM final concentration) in the presence of anti-CD107a antibody (clone 1D4B, BD Biosciences). The protein transport inhibitors brefeldin A and monensin (BD Biosciences) were added for the final 4 hours of restimulation. Stimulation with PMA/ionomycin (50 ng/ml PMA plus 2 μg/ml ionomycin, Sigma-Aldrich) served as a positive control. After restimulation, cells were surface stained for CD3ε (clone 145-2C11), CD8α, and CD19, followed by fixation/permeabilization and staining for intracellular IFN-γ (clone XMG1.2), TNF-α (clone MP6-XT22), and/or IL-2 (clone JES6-5H4) (all from BD Biosciences) and analyzed by flow cytometry. Background CD107a/cytokine levels following restimulation with an irrelevant peptide were subtracted from each experimental value.

Generation of bone marrow–derived DCs and immunizations

In preliminary experiments, we isolated primary pulmonary DCs from naive mice using magnetic selection with anti-CD11c microbeads (Miltenyi Biotec) and then peptide-loaded/LPS-matured them before immunizing recipient mice i.n. The purity of the isolated CD11c$^+$ DCs was 95%–98% and approximately 8%–10% were CD103$^+$ lung-resident DCs, which have been shown to efficiently home to draining LNs to prime naive T cells during respiratory virus infection (59). Intranasal immunization with 3 × 10^5 peptide-loaded, LPS-matured lung CD11c$^+$ DCs elicited unimpaired, PD-1^{lo} epitope-specific T$_{CD8}$ (data not shown). However, because of the need for large numbers of naive mice to obtain a sufficient quantity of pulmonary DCs, bone marrow–derived DCs were employed for all immunization experiments. Bone marrow–derived DCs were generated as previously described (79) with slight modifications. Briefly, bone marrow was obtained from the femurs and tibiae of B7tg mice, lysed of erythrocytes, and resuspended at 10^6 cells/ml in DC medium (R10 plus 20 ng/ml rmGM-CSF and 10 ng/ml rmIL-4 [Peprotech]) in 10-cm sterile tissue culture dishes. After 3 days of culture, 75% of the medium was replaced with fresh DC medium, and at day 6 cells were counted and replated. On day seven, 100 ng/ml LPS (Sigma-Aldrich) and 10 μM peptide were added overnight to mature and load the DCs with a particular epitope, respectively. The next day, DCs were collected, counted, and resuspended in PBS. By this time more than 85% of cells were CD11c^{hi} as determined by flow cytometry, which is characteristic of murine DCs. Maturation status was determined by staining unmatured or LPS-matured DCs for HLA-B*0702 (clone sc-53304, Santa Cruz Biotechnology Inc.), H2-IA^b (clone 25-9-17, BD Biosciences), CD86 (clone GL-1, BD Biosciences), CCR7 (eBioscience), CD11b (clone M1/70, BD Biosciences), and CD11c (clone HL3, BD Biosciences). For generation of lung-infiltrating epitope-specific T$_{CD8}$, mice were immunized i.n. with 2 × 10^6 peptide-loaded, LPS-matured DCs. Some mice were then challenged as described in the figure legends. Additionally, some mice immunized i.n. with M195-loaded DCs were treated daily i.n. with either 50 μg of M195 peptide or an irrelevant HLA-B*0702–restricted peptide. The same procedure was used to isolate lung lymphocytes from DC-immunized mice and virus-infected mice.

Real-time RT-PCR

Metal screens used for obtaining single-cell lymphocyte suspension from lungs (see above) were rinsed with 1 ml of RLT lysis buffer (QIAGEN), and the cell lysates were collected and frozen at –20°C. Samples were thawed and RNA was extracted using the MagNA Pure LC Total Nucleic Acid Isolation Kit (Roche Applied Sciences) on a MagNA Pure LC using the Total NA External Lysis protocol and stored at –80°C until further use. Real-time RT-PCR was performed in 2-μl reaction mixtures containing 5 μl of extracted RNA on an ABI StepOnePlus Real-Time PCR System (Life Technologies/Applied Biosystems) using the AgPath-ID One-Step RT-PCR kit (Applied Biosystems/Ambion). For HMPV genome detection, primers and probe targeting the HMPV N gene were previously published (80). Viral genome copy number was determined using a standard curve generated with RNA runoff transcripts of the target. For *PD-L1* gene expression, exon-spanning primers and probes were obtained and used according to the manufacturer's instructions (Applied Biosystems/Ambion). All values were normalized to the housekeeping gene *Hprt*, and experimental samples are reported as fold change in *PD-L1* compared with that in mice that were mock infected (100 μl i.n. of LLC-MK2 cell lysate) using the ΔΔCt method. Cycling conditions

were 50°C for 30 minutes, followed by an activation step at 95°C for 10 minutes and then 45 cycles of 15 seconds at 95°C, and 30 seconds at 60°C. Samples with Ct values less than 40 were considered positive.

PD-L blocking antibodies

Mice were injected i.p. with rat isotype control antibody (Bio X Cell, clone LTF-2) or both rat anti-mouse PD-L1 (Bio X Cell, clone 10F.9G2) and rat anti–mouse PD-L2 (Bio X Cell, clone TY-25) antibodies as described in the figure legends.

PD-L1 expression on human bronchial epithelial cells

The human bronchial epithelial cell line BEAS-2b was either mock infected with LLC-MK2 cell lysate or infected at various MOI with either HMPV or PR8 in serum-free Opti-MEM containing trypsin. Forty-eight hours later, cells were collected, LIVE/DEAD stained (see above), and then incubated with mouse anti–human PD-L1 antibody (clone MIH1, BD Biosciences) or isotype control for 30 minutes at 4°C. The fold increase in PD-L1 expression relative mock infection was determined by flow cytometry.

Immunohistochemistry of mouse and human lung specimens

Mouse. Mock- (i.e., LLC-MK2 cell lysate) or virus-infected lungs were inflated with 10% formalin and fixed overnight. Samples were then paraffin embedded and sectioned at 5-μm thickness before being placed on charged slides and baked overnight at 50°C. The paraffin was removed from the slides, and the sections were placed in heated Target Retrieval Solution (Dako) for 20 minutes. After an additional 20 minutes of cooling, the slides were rinsed in Tris-buffered saline–Tween for 5 minutes immediately prior to being placed on an automated Leica BOND-MAX IHC stainer. Endogenous peroxidase was neutralized with 0.03% hydrogen peroxide. Lungs were stained with anti-CD3 (Santa Cruz Biotechnology Inc.) for 60 minutes at room temperature. The Bond Intense R detection system was used for visualization.

Human. Tissue blocks obtained at autopsy from patients with confirmed LRI were provided by the Vanderbilt Translational Pathology Shared Resource with approval from the Vanderbilt Institutional Review Board (#111350). Influenza virus was detected by nasal swab in most cases and confirmed by lung H1N1 viral probe at the time of death. RSV infection was confirmed by rapid antigen testing. PIV-3 was confirmed by viral culture. Control lung specimens were obtained from individuals who expired from non-pulmonary disease. Patient characteristics are provided in the relevant figure legends. Samples were prepared as described above for mouse lungs. Anti–PD-L1 (clone 29E.2A3, BioLegend), anti–PD-1 (clone 7A11B1, Sigma-Aldrich), and anti-CD8 antibodies (clone C8/144B, Thermo Scientific) were used as the primary antibodies. The Bond Refine Polymer detection system was used for visualization. The slides were counterstained lightly with Mayer's hematoxylin, dehydrated, and coverslipped.

Pulse oximetry

A rodent pulse oximeter (MouseOx, Starr Life Sciences Corp.) was used to measure breath distension as previously described (81).

Statistics

Data analysis was performed using Prism version 4.0 (GraphPad Software). Comparisons between tetramer staining and ICS within the same animals were performed using a paired 2-tailed *t* test. Comparisons between 2 groups were performed using an unpaired 2-tailed Student's *t* test. Multiple group comparisons were performed using a 1-way ANOVA with a Bonferroni post-test for comparison of individual groups. A *P* values less than 0.05 was considered significant, with values of $P < 0.005$ and $P < 0.0005$ reported where applicable. Error bars in each graph represent SEM

Study approval

All animals were maintained in accordance with the *Guide for the Care and Use of Laboratory Animals* (NIH publication no. 85-23. Revised 1985) and were handled according to protocols approved by the Vanderbilt University Subcommittee on Animal Care (IACUC). The study involving analysis of human autopsy specimens was approved by the Vanderbilt University Institutional Review Board.

Acknowledgments

We thank D. Flaherty, B. Matlock, and K. Weller at the Vanderbilt Flow Cytometry Shared Resource and M. Rock and S. Yoder at the Vanderbilt Immunology Core for providing technical support and assistance with development of flow cytometry reagents. We also thank A. Sette, F. Lemonnier, and T. Honjo for providing mice used in these studies and J. McCullers for providing influenza virus strain HK/x31. This work was supported by AI085062 (to J.V. Williams), AI082417 (to J.V. Williams), AI040079 (to S. Joyce), AI042286 (to S. Joyce), HL054977 (to S. Joyce), and GM007347 for the Vanderbilt Medical Scientist Training Program (to J.J. Erickson). The VMC Flow Cytometry Shared Resource is supported by the Vanderbilt Ingram Cancer Center (P30 CA68485) and the Vanderbilt Digestive Disease Research Center (DK058404). This work was supported in part by Vanderbilt CTSA grant UL1 RR024975-01 from the National Center for Research Resources (NCRR)/NIH.

Received for publication January 12, 2012, and accepted in revised form June 7, 2012.

Address correspondence to: John V. Williams, 1161 21st Avenue South, D-7235 MCN, Nashville, Tennessee 37232-2581, USA. Phone: 615.936.2186; Fax: 615.343.9723; E-mail: john.williams@vanderbilt.edu.

1. Williams JV, et al. Human metapneumovirus and lower respiratory tract disease in otherwise healthy infants and children. *N Engl J Med*. 2004; 350(5):443–450.
2. Deffrasnes C, Hamelin ME, Boivin G. Human metapneumovirus. *Semin Respir Crit Care Med*. 2007;28(2):213–221.
3. Langley GF, Anderson LJ. Epidemiology and prevention of respiratory syncytial virus infections among infants and young children. *Pediatr Infect Dis J*. 2011;30(6):510–517.
4. Pavia AT. Viral infections of the lower respiratory tract: old viruses, new viruses, and the role of diagnosis. *Clin Infect Dis*. 2011;52(suppl 4):S284–S289.
5. Kroll JL, Weinberg A. Human metapneumovirus. *Semin Respir Crit Care Med*. 2011;32(4):447–453.
6. Johnson KM, Chanock RM, Rifkind D, Kravetz HM, Knight V. Respiratory syncytial virus. IV. Correlation of virus shedding, serologic response, and illness in adult volunteers. *JAMA*. 1961;176:663–667.
7. Hall CB, Walsh EE, Long CE, Schnabel KC. Immunity to and frequency of reinfection with respiratory syncytial virus. *J Infect Dis*. 1991;163(4):693–698.
8. Chang J, Braciale TJ. Respiratory syncytial virus infection suppresses lung CD8+ T-cell effector activity and peripheral CD8+ T-cell memory in the respiratory tract. *Nat Med*. 2002;8(1):54–60.
9. DiNapoli JM, Murphy BR, Collins PL, Bukreyev A. Impairment of the CD8+ T cell response in lungs following infection with human respiratory syncytial virus is specific to the anatomical site rather than the virus, antigen, or route of infection. *Virol J*. 2008;5:105.
10. Vallbracht S, Unsold H, Ehl S. Functional impairment of cytotoxic T cells in the lung airways following respiratory virus infections. *Eur J Immunol*. 2006;36(6):1434–1442.
11. Lukens MV, et al. Characterization of the CD8+ T cell responses directed against respiratory syncytial virus during primary and secondary infection in C57BL/6 mice. *Virology*. 2006;352(1):157–168.
12. Gray PM, Arimilli S, Palmer EM, Parks GD, Alexander-Miller MA. Altered function in CD8+ T cells following paramyxovirus infection of the respiratory tract. *J Virol*. 2005;79(6):3339–3349.
13. Bruder D, Srikiatkhachorn A, Enelow RI. Cellular immunity and lung injury in respiratory virus infection. *Viral Immunol*. 2006;19(2):147–155.
14. Jin HT, et al. Cooperation of Tim-3 and PD-1 in CD8 T-cell exhaustion during chronic viral infection. *Proc Natl Acad Sci U S A*. 2010;107(33):14733–14738.

15. Blackburn SD, et al. Coregulation of CD8+ T cell exhaustion by multiple inhibitory receptors during chronic viral infection. *Nat Immunol*. 2009;10(1):29–37.
16. Crawford A, Wherry EJ. The diversity of costimulatory and inhibitory receptor pathways and the regulation of antiviral T cell responses. *Curr Opin Immunol*. 2009;21(2):179–186.
17. Wherry EJ, Blattman JN, Murali-Krishna K, van der Most R, Ahmed R. Viral persistence alters CD8 T-cell immunodominance and tissue distribution and results in distinct stages of functional impairment. *J Virol*. 2003;77(8):4911–4927.
18. Blattman JN, Wherry EJ, Ha SJ, van der Most RG, Ahmed R. Impact of epitope escape on PD-1 expression and CD8 T-cell exhaustion during chronic infection. *J Virol*. 2009;83(9):4386–4394.
19. Barber DL, et al. Restoring function in exhausted CD8 T cells during chronic viral infection. *Nature*. 2006;439(7077):682–687.
20. Zhang JY, et al. PD-1 up-regulation is correlated with HIV-specific memory CD8+ T-cell exhaustion in typical progressors but not in long-term nonprogressors. *Blood*. 2007;109(11):4671–4678.
21. Velu V, et al. Elevated expression levels of inhibitory receptor programmed death 1 on simian immunodeficiency virus-specific CD8 T cells during chronic infection but not after vaccination. *J Virol*. 2007;81(11):5819–5828.
22. Sakuishi K, Apetoh L, Sullivan JM, Blazar BR, Kuchroo VK, Anderson AC. Targeting Tim-3 and PD-1 pathways to reverse T cell exhaustion and restore anti-tumor immunity. *J Exp Med*. 2010; 207(10):2187–2194.
23. Zhou Q, et al. Coexpression of Tim-3 and PD-1 identifies a CD8+ T-cell exhaustion phenotype in mice with disseminated acute myelogenous leukemia. *Blood*. 2011;117(17):4501–4510.
24. Inman BA, Frigola X, Dong H, Kwon ED. Costimulation, coinhibition and cancer. *Curr Cancer Drug Targets*. 2007;7(1):15–30.
25. Cheng X, Zhao Z, Ventura E, Gran B, Shindler KS, Rostami A. The PD-1/PD-L pathway is up-regulated during IL-12-induced suppression of EAE mediated by IFN-gamma. *J Neuroimmunol*. 2007;185(1–2):75–86.
26. Yamazaki T, et al. Expression of programmed death 1 ligands by murine T cells and APC. *J Immunol*. 2002;169(10):5538–5545.
27. Stanciu LA, Bellettato CM, Laza-Stanca V, Coyle AJ, Papi A, Johnston SL. Expression of programmed death-1 ligand (PD-L) 1, PD-L2, B7-H3, and inducible costimulator ligand on human respiratory tract epithelial cells and regulation by respiratory syncytial virus and type 1 and 2 cytokines. *J Infect Dis*. 2006;193(3):404–412.
28. Francisco LM, Sage PT, Sharpe AH. The PD-1 pathway in tolerance and autoimmunity. *Immunol Rev*. 2010;236:219–242.
29. Trautmann L, et al. Upregulation of PD-1 expression on HIV-specific CD8+ T cells leads to reversible immune dysfunction. *Nat Med*. 2006; 12(10):1198–1202.
30. Berger R, et al. Phase I safety and pharmacokinetic study of CT-011, a humanized antibody interacting with PD-1, in patients with advanced hematologic malignancies. *Clin Cancer Res*. 2008;14(10):3044–3051.
31. Brahmer JR, et al. Phase I study of single-agent anti-programmed death-1 (MDX-1106) in refractory solid tumors: safety, clinical activity, pharmacodynamics, and immunologic correlates. *J Clin Oncol*. 2010;28(19):3167–3175.
32. Zelinskyy G, et al. Virus-specific CD8+ T cells upregulate programmed death-1 expression during acute friend retrovirus infection but are highly cytotoxic and control virus replication. *J Immunol*. 2011;187(7):3730–3737.
33. Zhang Z, et al. Dynamic programmed death 1 expression by virus–specific CD8 T cells correlates with the outcome of acute hepatitis B. *Gastroenterology*. 2008;134(7):1938–1949.
34. Rutebemberwa A, et al. High-programmed death-1 levels on hepatitis C virus-specific T cells during acute infection are associated with viral persistence and require preservation of cognate antigen during chronic infection. *J Immunol*. 2008;181(12):8215–8225.
35. Phares TW, et al. Target-dependent B7-H1 regulation contributes to clearance of central nervous system infection and dampens morbidity. *J Immunol*. 2009;182(9):5430–5438.
36. Lafon M, et al. Detrimental contribution of the immuno-inhibitor B7-H1 to rabies virus encephalitis. *J Immunol*. 2008;180(11):7506–7515.
37. Lazar-Molnar E, Gacser A, Freeman GJ, Almo SC, Nathenson SG, Nosanchuk JD. The PD-1/PD-L costimulatory pathway critically affects host resistance to the pathogenic fungus Histoplasma capsulatum. *Proc Natl Acad Sci U S A*. 2008;105(7):2658–2663.
38. Huang X, et al. PD-1 expression by macrophages plays a pathologic role in altering microbial clearance and the innate inflammatory response to sepsis. *Proc Natl Acad Sci U S A*. 2009;106(15):6303–6308.
39. Yao S, et al. PD-1 on dendritic cells impedes innate immunity against bacterial infection. *Blood*. 2009;113(23):5811–5818.
40. Alvarez R, Tripp RA. The immune response to human metapneumovirus is associated with aberrant immunity and impaired virus clearance in BALB/c mice. *J Virol*. 2005;79(10):5971–5978.
41. Melendi GA, et al. Mapping and characterization of the primary and anamnestic H-2(d)-restricted cytotoxic T-lymphocyte response in mice against human metapneumovirus. *J Virol*. 2007;81(20):11461–11467.
42. Williams JV, Tollefson SJ, Johnson JE, Crowe JE Jr. The cotton rat (Sigmodon hispidus) is a permissive small animal model of human metapneumovirus infection, pathogenesis, and protective immunity. *J Virol*. 2005;79(17):10944–10951.
43. Rohrlich PS, et al. HLA-B*0702 transgenic, H-2KbDb double-knockout mice: phenotypical and functional characterization in response to influenza virus. *Int Immunol*. 2003;15(6):765–772.
44. Horton H, et al. Correlation between interferon-gamma secretion and cytotoxicity, in virus-specific memory T cells. *J Infect Dis*. 2004;190(9):1692–1696.
45. Betts MR, et al. Sensitive and viable identification of antigen-specific CD8+ T cells by a flow cytometric assay for degranulation. *J Immunol Methods*. 2003;281(1-2):65–78.
46. Flynn KJ, Belz GT, Altman JD, Ahmed R, Woodland DL, Doherty PC. Virus-specific CD8+ T cells in primary and secondary influenza pneumonia. *Immunity*. 1998;8(6):683–691.
47. Hamilton SE, Harty JT. Quantitation of CD8+ T cell expansion, memory, and protective immunity after immunization with peptide-coated dendritic cells. *J Immunol*. 2002;169(9):4936–4944.
48. Badovinac VP, Messingham KA, Jabbari A, Haring JS, Harty JT. Accelerated CD8+ T-cell memory and prime-boost response after dendritic-cell vaccination. *Nat Med*. 2005;11(7):748–756.
49. Roberts AD, Woodland DL. Cutting edge: effector memory CD8+ T cells play a prominent role in recall responses to secondary viral infection in the lung. *J Immunol*. 2004;172(11):6533–6537.
50. Kinter AL, et al. The common gamma-chain cytokines IL-2, IL-7, IL-15, and IL-21 induce the expression of programmed death-1 and its ligands. *J Immunol*. 2008;181(10):6738–6746.
51. Keir ME, Butte MJ, Freeman GJ, Sharpe AH. PD-1 and its ligands in tolerance and immunity. *Annu Rev Immunol*. 2008;26:677–704.
52. Mueller SN, Ahmed R. High antigen levels are the cause of T cell exhaustion during chronic viral infection. *Proc Natl Acad Sci U S A*. 2009; 106(21):8623–8628.
53. Hartert TV, Wheeler AP, Sheller JR. Use of pulse oximetry to recognize severity of airflow obstruction in obstructive airway disease: correlation with pulsus paradoxus. *Chest*. 1999;115(2):475–481.
54. Rebuck AS, Pengelly LD. Development of pulsus paradoxus in the presence of airways obstruction. *N Engl J Med*. 1973;288(2):66–69.
55. Nishimura H, Minato N, Nakano T, Honjo T. Immunological studies on PD-1 deficient mice: implication of PD-1 as a negative regulator for B cell responses. *Int Immunol*. 1998;10(10):1563–1572.
56. Telcian AG, et al. RSV-induced bronchial epithelial cell PD-L1 expression inhibits CD8+ T cell nonspecific antiviral activity. *J Infect Dis*. 2011;203(1):85–94.
57. Velu V, et al. Enhancing SIV-specific immunity in vivo by PD-1 blockade. *Nature*. 2009;458(7235):206–210.
58. Schwarze J, O'Donnell DR, Rohwedder A, Openshaw PJ. Latency and persistence of respiratory syncytial virus despite T cell immunity. *Am J Respir Crit Care Med*. 2004;169(7):801–805.
59. Kim TS, Hufford MM, Sun J, Fu YX, Braciale TJ. Antigen persistence and the control of local T cell memory by migrant respiratory dendritic cells after acute virus infection. *J Exp Med*. 2010;207(6):1161–1172.
60. Paulsson KM, Wang P. Quality control of MHC class I maturation. *FASEB J*. 2004;18(1):31–38.
61. Bucks CM, Norton JA, Boesteanu AC, Mueller YM, Katsikis PD. Chronic antigen stimulation alone is sufficient to drive CD8+ T cell exhaustion. *J Immunol*. 2009;182(11):6697–6708.
62. Mueller SN, et al. PD-L1 has distinct functions in hematopoietic and nonhematopoietic cells in regulating T cell responses during chronic infection in mice. *J Clin Invest*. 2010;120(7):2508–2515.
63. Rodriguez-Garcia M, et al. Expression of PD-L1 and PD-L2 on human macrophages is up-regulated by HIV-1 and differentially modulated by IL-10. *J Leukoc Biol*. 2011;89(4):507–515.
64. Pellegrini M, et al. IL-7 engages multiple mechanisms to overcome chronic viral infection and limit organ pathology. *Cell*. 2011;144(4):601–613.
65. Chang J, Choi SY, Jin HT, Sung YC, Braciale TJ. Improved effector activity and memory CD8 T cell development by IL-2 expression during experimental respiratory syncytial virus infection. *J Immunol*. 2004;172(1):503–508.
66. Youngblood B, et al. Chronic virus infection enforces demethylation of the locus that encodes PD-1 in antigen-specific CD8(+) T cells. *Immunity*. 2011;35(3):400–412.
67. West EE, et al. Tight regulation of memory CD8(+) T cells limits their effectiveness during sustained high viral load. *Immunity*. 2011;35(2):285–298.
68. Kim J, et al. Constitutive and inducible expression of b7 family of ligands by human airway epithelial cells. *Am J Respir Cell Mol Biol*. 2005;33(3):280–289.
69. Heinecke L, Proud D, Sanders S, Schleimer RP, Kim J. Induction of B7-H1 and B7-DC expression on airway epithelial cells by the Toll-like receptor 3 agonist double-stranded RNA and human rhinovirus infection: in vivo and in vitro studies. *J Allergy Clin Immunol*. 2008;121(5):1155–1160.
70. Rock MT, McKinney BA, Yoder SM, Prudom CE, Wright DW, Crowe JE Jr. Identification of potential human respiratory syncytial virus and metapneumovirus T cell epitopes using computational prediction and MHC binding assays. *J Immunol Methods*. 2011;374(1–2):13–17.
71. Rock MT, Crowe JE Jr. Identification of a novel human leucocyte antigen-A*01-restricted cytotoxic T-lymphocyte epitope in the respiratory syncytial virus fusion protein. *Immunology*. 2003; 108(4):474–480.
72. Choi EY, et al. Quantitative analysis of the immune response to mouse non-MHC transplantation antigens in vivo: the H60 histocompatibility antigen dominates over all others. *J Immunol*. 2001; 166(7):4370–4379.
73. Rodenko B, et al. Generation of peptide-MHC class I complexes through UV-mediated ligand

exchange. *Nat Protoc*. 2006;1(3):1120–1132.
74. Bakker AH, et al. Conditional MHC class I ligands and peptide exchange technology for the human MHC gene products HLA-A1, -A3, -A11, and -B7. *Proc Natl Acad Sci U S A*. 2008;105(10):3825–3830.
75. Toebes M, Rodenko B, Ovaa H, Schumacher TN. Generation of peptide MHC class I monomers and multimers through ligand exchange. *Curr Protoc Immunol*. 2009;Chapter 18:Unit 18.16.
76. Hadrup SR, et al. High-throughput T-cell epitope discovery through MHC peptide exchange. *Methods Mol Biol*. 2009;524:383–405.
77. Lissina A, et al. Protein kinase inhibitors substantially improve the physical detection of T-cells with peptide-MHC tetramers. *J Immunol Methods*. 2009;340(1):11–24.
78. Yuen TJ, et al. Analysis of A47, an immunoprevalent protein of vaccinia virus, leads to a reevaluation of the total antiviral CD8+ T cell response. *J Virol*. 2010;84(19):10220–10229.
79. Matheu MP, Sen D, Cahalan MD, Parker I. Generation of bone marrow derived murine dendritic cells for use in 2-photon imaging. *J Vis Exp*. 2008;(17):773.
80. Ali SA, et al. Real-world comparison of two molecular methods for detection of respiratory viruses. *Virol J*. 2011;8:332.
81. Stokes KL, et al. Differential pathogenesis of respiratory syncytial virus clinical isolates in BALB/c mice. *J Virol*. 2011;85(12):5782–5793.